Live Rekvig

Effect of surfactant structure on properties of oil/water interfaces. A coarse-grained molecular simulation study.

Doctoral thesis submitted to
Department of Chemistry
Norwegian University of Science and Technology
in partial fulfillment of the requirements
for the PhD degree.

Trondheim, October 2004

ISBN 82-471-6511-2 (printed version)
ISBN 82-471-6510-4 (electronic version)

Acknowledgement

The research presented here was conducted in 2001–2004 in the Department of Chemistry, Norwegian University of Science and Technology (NTNU), under supervision of Prof. Bjørn Hafskjold, with several extended stays in the group of Prof. Berend Smit in the Department of Chemical Engineering in the University of Amsterdam. The project was funded by the Research Council of Norway, VISTA, and NTNU. Computations were performed on high performance computers provided by the Physical Chemistry section at NTNU and by the Norwegian High Performance Computing Consortium (NOTUR).

These four years have given me a unique opportunity to work long-term on a very interesting topic, and a lot of freedom to dwell with whatever I found interesting. But doing a PhD is also sometimes lonely and frustrating. Fortunately, the help and support from supervisors, colleagues, and friends have eased the pain considerably.

First I would like to thank my supervisor, Bjørn Hafskjold, for his wise advice, scientific and career-wise, for always taking time when I needed help, and for never hesitating to go out of his way to help me further my research career.

I am also very grateful to Berend Smit for accepting me into his group, first for a year in 2002 during my supervisor's sabbatical in Japan, then for many shorter and longer stays during the last two years. He treated me as one of his own students and his constant enthusiasm and inspiration have been very important for my work.

Øystein Sæther, postdoc in our group in the first year of my PhD work, taught me about surfactants and interfacial phenomena, which was quite new for me then, but actually quite interesting.

I also thank all my colleagues in the Physical Chemistry group in Trondheim and in the Computational Physics and Chemistry group in Amsterdam. In particular, Marieke for teaching me DPD and being coauthor of two papers, David for sharing his knowledge on computers and simulations so generously, Lars, Martin, Audun, and Einar for maintaining the local computer facilities, and Terje for allocating the money for it.

Now it feels like very long ago, but I want to thank Letten F. Saugstad and Peter Derlet whose encouragement made me apply for a PhD in the first place. Finally, I want to thank my parents and brothers for showing that they are proud of me, and dearest Gadi for all the encouragement with the papers, and for everything else.

Summary

The elastic properties of oil/water/surfactant interfaces play an important role in the phase behaviour of microemulsions and for the stability of macroemulsions. The aim of this thesis is to obtain an understanding of the relationship between the structure of the surfactant molecules, the structure of the interface, and macroscopic interfacial properties. To achieve this aim, we performed molecular simulations of oil/water/surfactant systems. We made a quantitative comparison of various model surfactants to determine how structural changes affect interfacial properties and film rupture. The model consists of water, oil, head, and tail beads, and surfactants are constructed by coupling head and tail beads with harmonic springs. We used a hybrid dissipative particle dynamics-Monte Carlo scheme. The former was used to simulate particle trajectories and the Monte Carlo scheme was used to mimic experimental conditions: bulk-interface phase equilibrium, tensionless interfaces in microemulsions, and the surface force apparatus.

A detailed comparison of various non-ionic model surfactants showed how structural changes affect interfacial properties:

Comparison between linear and branched surfactants showed that the efficiency of adsorption is higher for linear surfactants, although branched surfactants are more efficient at a given surface density. Linear surfactants can be more efficient also at the same surface density if the head group is sufficiently soluble in oil, because low head-oil repulsion makes the branched isomers stagger at the interface. The bending rigidity is higher for linear surfactants. Furthermore, branched surfactants make oil droplets coalesce more easily than linear surfactants do, but linear and branched surfactants have roughly the same effect on water droplet coalescence.

Comparison of linear surfactants with varying chain lengths showed that longer surfactants have a lower surface tension and higher bending rigidity. The increase in rigidity with chain length follows a power law, but the exponent is higher for surfactant monolayers at a fixed density than at a fixed tension. Longer tails and/or denser monolayers influence the stability of water droplets in a positive direction, and the stability of oil droplets in a negative direction.

Addition of cosurfactant showed that mixed monolayers have a lower bending rigidity than pure monolayers at the same average chain length and tension. Cosurfactants have a negative effect on the stability of water droplets, and a positive effect on the stability of oil droplets.

Nomenclature

Here follows an overview of notation used in chapters 1–5. Abbreviations and symbols which are used only in the paragraph where they are defined are not included here. Also, symbols used only in papers I–V are not included here, but are defined in each paper.

Abbreviations

CMC	critical micelle concentration
DPD	dissipative particle dynamics
MC	Monte Carlo
MD	molecular dynamics
μVT	constant chemical potential, volume, and temperature
NγVT	constant number of particles, interfacial tension, volume, and temperature
NPT	constant number of particles, pressure, and temperature
NVE	constant number of particles, volume, and energy
NVT	constant number of particles, volume, and temperature

Symbols

Latin letters

A	area
a	DPD repulsion parameter
$\bar{c}$	average curvature
c_0	spontaneous (natural) curvature
c_1, c_2	principal curvatures
c	concentration (N_{surf}/V)
E	energy
$\mathbf{F}$	force
$\mathbf{F}_i$	force on particle i
$\mathbf{F}_{ij}$	force on particle i exerted by particle j
G	Gibbs free energy

h	local height of the interface
$\tilde{h}$	Fourier transform of h
k_B	Boltzmann's constant
k_s	spring constant in the bond potential
L	box length
m	mass
N	number of particles
N_m	number of water molecules per DPD bead
n	new (Monte Carlo configuration)
o	old (Monte Carlo configuration)
P	probability
P	pressure
p	exponent in power law
p_α	pressure in direction α
q	2π/undulation wave length
r	inter-particle distance
r_0	bond length which minimizes U^{bond}
r_c	cut-off value for the interactions
$\mathbf{r}_i$	position of particle i
$\mathbf{r}_{ij}$	$\mathbf{r}_i - \mathbf{r}_j$
r_{ij}	$\lvert\mathbf{r}_{ij}\rvert$
$\hat{\mathbf{r}}_{ij}$	$\mathbf{r}_{ij}/r_{ij}$
$\mathbf{r}^N$	$\mathbf{r}_1, \mathbf{r}_2, \cdots, \mathbf{r}_N$
$\mathbf{dr}^N$	$\mathbf{dr}_1 \cdot \mathbf{dr}_2 \cdots \mathbf{dr}_N$
T	temperature
t	time
U	potential energy
V	volume
$\mathbf{v}_i$	velocity of particle i
$\mathbf{v}_{ij}$	$\mathbf{v}_i - \mathbf{v}_j$
w	weight function

Greek letters

β	$k_B T$
Γ	surface excess adsorption
γ	interfacial tension
γ_0	oil/water interfacial tension without surfactants
Δ	increment, difference
η	amplitude of the dissipative force
θ	gaussian random number
κ	mean bending modulus

$\bar{\kappa}$	saddle splay modulus
λ	integration parameter
μ	chemical potential
ρ	density (N/V)
σ	amplitude of the random force

Subscripts and superscripts

α	direction (x, y or z)
C	conservative
D	dissipative
em	equimolar
h	head
i, j, k	particle numbers
o	oil
R	random
surf	surfactant
t	tail
w	water

Contents

Chapter 1

Introduction

1.1 Surfactant monolayers at oil/water interfaces

Anyone who tried to mix olive oil and balsamic vinegar, or tried to clean greasy dinner plates without soap, knows that oil (fat) and water do not mix easily. Nevertheless, such mixtures are abundant in both nature and industrial products. A stable dispersion of one liquid in a second immiscible liquid is called an emulsion. Milk and mayonnaise are examples from daily life; milk is an oil-in-water emulsion, and mayonnaise is a water-in-oil emulsion. The fat droplets in milk are 0.1–10 micrometer in diameter, but in other emulsions the droplets can be up to a millimeter large. What prevents emulsions from separating right away is the presence of surfactants. Surfactants are amphiphilic molecules that adsorb on the oil/water interface and form oriented monolayers with the hydrophilic part in the water phase and the hydrophobic part in the oil phase.

Surfactants are involved in many processes throughout industry. There is an enormous interest in the behaviour of surfactants, and especially in designing the optimal surfactant for a given problem. Unfortunately, this task is extremely complex. Emulsions are in general thermodynamically unstable, even with surfactant present. The separation kinetics, however, depend on many factors. Thus, it is sometimes a challenge to stabilise emulsions sufficiently long for the required lifetime, and sometimes a challenge to destabilise an undesired emulsion. Separation occurs via flocculation, creaming, or sedimentation, followed by droplet coalescence, and the stability depends on the rate of these processes. Some determining factors are the properties of the continuous phase, the interaction between droplets, droplet size distribution, and the elastic properties of the oil/water interface. The latter depend largely on the specific properties of the actual surfactant.

Microemulsions are emulsions that are thermodynamically stable. They have a high surfactant content and ultra-low interfacial energies. Only certain surfactants can form microemulsions, and usually a mixture of several types is needed. Microemulsions have droplet sizes of only 10–200 nm or are bi-continuous. They are totally dominated by interfaces and their phase behaviour is determined by the

properties of the surfactant films to an even greater extent than macroemulsions.

1.2 Revealing the connection between surfactant structure and macroscopic properties

Surfactant and emulsion science have a long history. In some sense, surfactant science is a reasonably mature science [1]. However, practical emulsion science is very complex, and new applications and new challenges arise continuously in this field [2]. The more recent interest in microemulsions, liquid crystals, and lipid membranes has greatly improved the general understanding of liquid interfaces, and this has also had an impact on the understanding of macroemulsions.

For a long time, emulsion science was empiric and phenomenological. The Bancroft rule, the Griffin HLB (hydrophilic-lipophilic balance) scale, and the Shinoda phase-inversion concept stem from this period [3]. These still serve as rules of thumb when predicting whether a given surfactant will stabilise oil-in-water or water-in-oil emulsions.

The classical DLVO-theory is the main ingredient in an approach to explain emulsion stability in terms of inter-droplet forces, or the so-called disjoining pressures [4]. This theory describes the van der Waals and electrostatic forces between droplets covered by ionic surfactants. With non-ionic surfactants, steric forces are important. Forces between two interfaces can be elegantly measured with the surface force apparatus [5]. This has revealed a number of other surface forces such as depletion, oscillatory structural forces, protrusion and undulation forces. The latter two are due to thermal fluctuations in the interface, and are important in microemulsions and bilayers where the interfacial tension is low [6].

Microemulsions are now fairly well understood in terms of their elastic constants [7,8]: the interfacial tension, γ, the mean and saddle splay bending moduli, κ and $\bar{\kappa}$, and the spontaneous curvature of the surfactant monolayer, c_0. It is generally accepted that knowledge of the equilibrium phase behaviour of oil/water/surfactant mixtures is essential for understanding microemulsions [9]. The connection between macroemulsion stability and phase equilibria is, however, less explored. Recently it was shown that the bending rigidity and spontaneous curvature affect the coalescence rate via the coalescence channel free energy [10]. This affirms that the interfacial elastic properties play an important role also in macroemulsions.

To complete the picture, one needs an understanding of how the interfacial properties depend on the detailed structure of the surfactant. The interfacial tension is perhaps the most important property of an interface. Classic methods to measure the surface tension at a liquid/vapour interface are the Langmuir trough and the Wilhelmy plate methods [11]. If the surfactants have low bulk solubility, the Langmuir trough gives pressure-area isotherms for the surfactant film. Otherwise, the surface tension plotted versus the bulk concentration gives the critical micelle concentration, at the sharp knee in the curve. Surface tension measurements at

the oil/water interface can be conducted with the pendant drop or spinning drop techniques [12].

More recently, light, X-ray, and neutron scattering experiments have enabled a more detailed study of the structure of the interface [13, 14]. From scattering spectra one can also extract the mean bending modulus of a liquid/gas interface [13]. Both the mean and saddle splay bending moduli can be estimated from scattering experiments on bulk microemulsions [8, 15].

A mean-field theory for amphiphilic mono- and bilayers was developed by Szleifer et al [16–18]. They calculated the elastic properties as well as detailed chain packing statistics of surfactant monolayers of various compositions.

Molecular simulations often provide a link between theory and experiment. The first simulations of model surfactants at oil/water interfaces appeared at the end of the 1980s [19]. This bead-spring model of hydrophilic and hydrophobic beads forms the basis for many current models. With the rapid increase in computer power, all-atom models have become feasible for some cases. On the other hand, the desire to reach mesoscopic time and length scales drives the development of coarse-grained models. Molecular simulations have been used to study self-assembled surfactant monolayers [20–24], micelle formation in bulk [25–27], and the solubilisation of oil into (swollen) micelles [28].

From the large record of experiments, theory, and simulations in this area one can extract some general trends [29]: The surface tension is reduced more efficiently with longer surfactants, with linear rather than branched surfactants, and with non-ionic rather than ionic surfactants. However, there are exceptions, for example are some branched surfactants more efficient than their linear isomers. The mean bending modulus is of the order of a few k_BT for monolayers and 10–100k_BT for bilayers. It increases with surfactant tail length n with a power law $\kappa \propto n^p$. The reported values of p typically lie around 2–3. Addition of a cosurfactant reduces κ.

1.3 Scientific objective

The principal aim of this thesis is to contribute to the understanding of the role of surfactants at oil/water interfaces. The present record of surfactant structure-performance relationship is to a large extent based on experience. Much is known, but a better understanding of the underlying mechanisms would facilitate the process of choosing or developing the optimal surfactant for a given application.

The interfacial tension and the mean bending modulus can be measured readily in experiments. However, obtaining a molecular understanding of the measured properties is difficult because one does not know the molecular structure of the interface. Obtaining such information is usually impossible, or requires expensive experiments at large facilities, e.g. neutron scattering.

In contrast, molecular simulations can be used not only to compute interfacial properties, but also to obtain detailed information about density profiles, packing, and alignment of surfactants at the interface. Furthermore, one can systematically

vary parameters and conditions such as the surface density or bulk concentration of surfactant, the surfactant tail length, head group size, tail branching, and the head and tail affinities for oil and water.

The aim of this thesis is thus to obtain an understanding of the relation between the structure of the molecules, the structure of the interface, and macroscopic, measurable properties. Specifically, we address the following questions: Why do branched surfactants reduce γ sometimes more and sometimes less efficiently than their linear isomers? What property and mechanism are determining? Is the higher efficiency due to a stronger adsorption at the interface, or stronger interactions between the surfactants that are at the interface? Furthermore, how is the bending modulus affected by variations in chain length, branching, and concentration of co-surfactant? What is the value of the exponent p? Is it universal, and under what conditions? And finally, can we create a simple system that enables an equally systematic study of the effect of surfactant structure on droplet stability in emulsions?

1.4 Outline of the thesis

The core of this thesis is five papers that are published, or accepted for publication, in peer-reviewed international journals. These are included at the end, in the order that they were written. Each paper can be read independently.

Chapters 2, 3, and 4 serve as background information. Chapter 2 is an introduction to surfactants and emulsions. Chapter 3 gives an introduction to molecular simulations, provides a justification of the choice of model and method, and discusses some details on the simulations that were omitted in the papers. Chapter 4 contains a brief introduction to fluid interfaces and discusses some of the choices made in the treatment of the simulation data. Chapter 5 contains conclusions and outlook.

Papers I and II show how the interfacial tension depends on the surface density and bulk concentration. Paper I is a letter containing only the most important results. Paper II also contains an extensive discussion of the relation between surfactant structure and interfacial tension as well as a description of a method to simulate bulk-interface equilibria. This work presents two important results: The first is concerned with the difference between linear and branched surfactants, where we showed that the head-oil solubility determines whether the linear or branched isomers reduce γ more. The head-oil interaction determines the packing at the interface, which again determines the lateral interactions and interfacial tension. A detailed analysis of the packing at the interface was necessary to understand these results.

The second result is related to the experimental concept 'efficiency of adsorption'. We found that the bulk concentration needed to obtain a given interfacial tension is lower with linear surfactants than with branched surfactants. This is also observed experimentally, but we provided an explanation: Although branched surfactants reduce the interfacial tension more efficiently (given the same surface

density), the adsorption is lower than for linear surfactants, giving a lower interfacial tension at the same bulk concentration.

In paper III we computed the mean bending modulus for pure and mixed monolayers. Also here, we perform a detailed comparison between different structures. Most of the comparisons are made at a fixed, low, interfacial tension, to mimic the flexible interfaces in microemulsions. Paper IV is a detailed study of the chain length dependence of the bending modulus. The main result here is that the exponent in the power law depends on whether the monolayers have a fixed interfacial density or fixed interfacial tension. This resolves, in part, some earlier experimental and theoretical discrepancies.

Whereas papers I–IV present interfacial properties of single oil/water/surfactant interfaces, we moved to interacting interfaces in paper V. This paper shows force-distance curves for two approaching interfaces. The qualitative difference between oil/water/oil films and water/oil/water films is attributed to the spontaneous curvature of the surfactant monolayer. We also detect the distance at which film rupture occurs and provide a qualitative comparison between different structures.

Papers II, III, and V all introduce new ways of simulating oil/water/surfactant interfaces. These papers describe sophisticated simulation systems, and although the techniques themselves are well-known, the particular applications are original. In every case, the underlying motivation is to create simulation systems that mimic the experimental conditions. Thus, part of the present contribution is to show how advanced simulations can be used to study surfactant monolayers.

Chapter 2

Surfactants and their applications

2.1 Surfactants

Surfactants form a unique class of molecules [1, 29]. The name is short for 'surface active agents'. They are surface active because they have both hydrophilic and lipophilic (hydrophobic) groups, typically an oil-soluble hydrocarbon chain and a water-soluble ionic or polar group. Their presence radically alters the properties of many surfaces and interfaces.

2.1.1 Behaviour

Surfactants behave quite similarly on air/water and oil/water interfaces. We will first illustrate the basic behaviour with air as the non-polar phase. Figure 2.1 shows a schematic drawing of self-assembling surfactants. Even at very low concentrations, the surfactants tend to adsorb on the interface and orient with their heads in the water and tails in the air. The reason for this is two-fold: It minimises the unfavourable interaction between water and the hydrophobic tails, and it reduces the interfacial tension of the air/water interface.

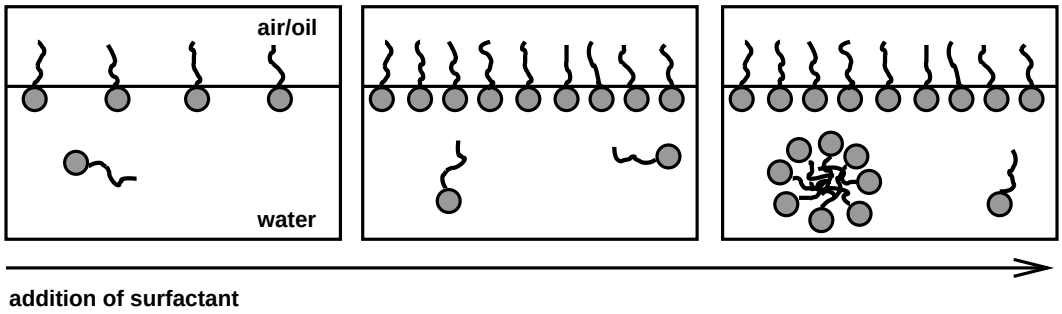

Figure 2.1: Cartoon of the self-assembly of surfactants into a monolayer on air/water (or oil/water) interfaces, and into micelles at concentrations higher than the critical micelle concentration.

The surface properties change smoothly with increasing concentration of surfactant, but only up to a certain point. Further addition of surfactant has almost no effect on the interfacial properties. Instead, the properties of the bulk phase change radically, e.g. a high increase in viscosity. This is because surfactants self-assemble into micelles – spherical aggregates in which the tails are in the interior, shielded from the water by the head groups. The concentration where this occurs is called the critical micelle concentration (CMC).

Micelles coexist with single surfactants, but the distribution of aggregate sizes is fairly sharp with a maximum at around 50–100 surfactants per micelle [1]. Depending on the surfactant structure and concentration, the micelles can grow to form hexagonally packed rods (worm-like micelles), or lamellae (liquid crystals).

A similar behaviour is observed at oil/water interfaces. At low concentrations, the surfactants adsorb on the interface. At higher concentrations, the equilibrium phase behaviour of oil/water/surfactant systems is very rich. Possible structures are micelles in water, inverse micelles in oil, swollen (inverse) micelles or microemulsion droplets, bi-continuous structures and lamellae. Very simplified, the phase behaviour can be understood by ascribing a molecular packing parameter $v/(al)$ to the surfactants, where a is the optimum head group area, v is the effective hydrocarbon volume, and l is the fully extended chain length [30]. The packing parameter depends on the molecular structure as well as the effective interactions between the various hydrophilic and hydrophobic groups and the surroundings. For example, an increase in temperature will increase v while addition of salt will decrease a for ionic surfactants. Thus, the packing parameter describes the effective shape of the surfactant, see Figure 2.2. A low value gives micelles in water coexisting with oil. Upon increase in the packing parameter, the micelles become swollen with oil. Balanced surfactants may form swollen lamellae or bi-continuous structures and an even higher packing parameter gives (swollen) inverse micelles in the oil phase.

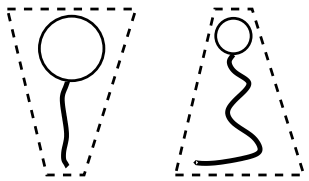

Figure 2.2: Cartoon of two surfactants with a low (left) and high (right) packing parameter, respectively. The left one will tend to form micelles in the water phase, and the right will tend to form inverse micelles in the oil phase.

2.1.2 The hydrophobic effect

Surfactants self-assemble into monolayers at interfaces and into micelles in bulk water in order to avoid contact between hydrocarbon chains and water. This is known as the hydrophobic effect [31]. Its microscopic origin is still a matter of

investigation [32], but it is believed to be entropic rather than energetic. Attractive dispersion forces act between alkyl groups and water as well as between two alkyl groups. However, presence of a non-polar moiety interrupts the hydrogen-bonded structure of water. According to the 'iceberg theory', water tends to form ordered cages around the non-polar molecule, leading to a decrease in entropy. Self-assembly minimises this effect. Recent simulations and experiments did not confirm such 'icebergs', but it is clear that the hydrophobic effect is due to the high free energy of cavity creation in water compared to organic solvents [33].

2.1.3 Classification of surfactants

Surfactants are classified according to their head groups. Anionic, cationic, zwitterionic (having both anionic and cationic groups), and non-ionic. During the last twenty years, much attention has been devoted to Gemini surfactants [26,34]. These are comprised of two heads and two tails, plus a spacer between the two heads. The tendency for Gemini surfactants to adsorb at interfaces, rather than form micelles, is much higher than for conventional surfactants [34]. Depending on the application, this may or may not be desired.

There are other surface active compounds in addition to classic surfactants: Polymers, polyelectrolytes, lipids, proteins, macromolecules, and solid aggregates may also show some surface active behaviour. Compared to these, surfactants are relatively small molecules. Surfactants are also the only class of molecules that forms micelles. This thesis will deal only with classic molecular surfactants.

Surfactants are also called amphiphiles, but not all amphiphilic molecules are considered surfactants. Alcohols, for example, are amphiphilic, and can serve as cosurfactant, but are not sufficiently surface active on their own to classify as surfactants. Surfactants may therefore be defined as amphiphiles which form oriented monolayers at interfaces.

In classical surfactant science, the following properties are used to quantify surfactant performance:

- Efficiency, or efficiency of adsorption, is quantified by $\mathrm{pC}_{20} \equiv -\log_{10} C_{20}$, where C_{20} is the bulk concentration of surfactant required to reduce the surface tension γ by 20mN/m ($\gamma \approx 70$mN/m for an air/water interface without surfactant).

- CMC: The critical micelle concentration is the bulk concentration at which micelle formation begins.

- Effectiveness: The surface tension at CMC. This is usually the minimal possible surface tension.

Rosen [29] lists some structural changes that in general increase the efficiency of a surfactant: increased number of CH_2 groups, linear rather than branched chain, and decreased effective charge of the head group. In papers I–II we discuss how

the efficiency depends both on the adsorption and on the interaction between the adsorbed molecules.

2.1.4 Applications

Surfactants form an integral part of our life: Personal care products like soaps, creams, shampoos, and detergents would not work without surfactants. Milk, butter, ice-cream, sauces, and dressings are stabilised by (natural) surfactants. The membranes of all living cells consist of amphiphilic bilayers, and surfactants are present at the air/liquid interfaces in the lungs. Surfactants are involved in many industrial processes, added for a purpose or as an undesired side-effect. Many surfactant applications fall into one of the following categories [1]:

- Detergency. Surfactants are the active components in soap and detergents. Their ability to dissolve fat, oil, and dirt into water is a direct result of their adsorption at such interfaces.
- Stabilisation and destabilisation of colloidal dispersions, e.g. foams, emulsions, and suspensions. Surfactants that stabilise emulsions are also referred to as emulsifiers. Emulsifiers are used in the food, cosmetics, and pharmaceutical industries, as well as in paints, pesticides and other chemical products [35]. Surfactants can also speed up the separation of undesired emulsions by counteracting the stabilising compounds (often macromolecules or solid aggregates). This is exploited e.g. in the oil industry, and such surfactants are referred to as demulsifiers.
- Wettability alteration. Surfactants that adsorb on solid/liquid interfaces modify the ability of oil or water to wet the solid surface. They can make water-wetting surfaces oil-wetting, and vice versa. Addition of surfactant may therefore facilitate displacement of liquids through porous media, e.g. drive oil out of sandy rocks.
- Micelles provide small compartments with a well-defined size. State-of-the-art in therapeutic drug delivery is storage of oil soluble and water soluble compounds into micelles and vesicles, respectively, for controlled release at the appropriate part of the body. Micelles can also be used as microreactors.

2.2 Oil/water emulsions

Oil and water do not mix easily. To create a dispersion of oil droplets in water or vice versa, energy, e.g. shear forces, must be applied. When the shaking or stirring stops, the dispersion will separate via droplet flocculation, sedimentation, or creaming, followed by coalescence. Separation occurs because of the high interfacial tension between oil and water, but the tension can be significantly reduced by adding

surfactants. The surfactants can slow down the separation process enough to make the dispersion practically stable (i.e. during the required life time). It is then referred to as an emulsion. Emulsion droplets are typically 0.1–100 micrometers in diameter, implying a very large total interfacial area. Their stability is usually only kinetic, not thermodynamic.

Surfactants influence emulsion stability in several ways: They alter the properties of the continuous phase and thereby the droplet collision rate, the effective droplet-droplet interactions, and the elastic properties of the interfacial film. This makes emulsion stability a very complex field [2].

In practice, separation of undesired emulsions can be very challenging. This is the case in the petroleum industry, where co-produced water must be removed from the oil for further processing, and oil must be removed from waste water for environmental reasons. These emulsions are stabilised by natural surfactants or larger surface-active compounds (macromolecules or solid aggregates). A demulsifier, a different surfactant which promotes flocculation and/or coalescence, may be added to aid the separation. The added surfactant may replace the natural emulsifier, or otherwise break the stabilising film.

2.3 Microemulsions

Microemulsions are emulsions that are thermodynamically stable [36]. They are characterised by ultra-low interfacial tensions, obtained with high concentrations of surfactant, and usually a cosurfactant. The droplet sizes are significantly smaller than in regular emulsions (hence the name), but other structures can coexist: Bicontinuous, cubic structures (oil- and water-continuous), and sponge-like structures (cubic bilayers). Structure exists only on the microscopic scale, with continuous transitions and very dynamic interfaces. The widespread interest in microemulsions owe to their extremely large interfacial areas, ultra-low tension, and high capacity to solubilise both hydrophilic and hydrophobic compounds.

To understand the rich structural variations and transitions in microemulsions, the flexible surface model has proved successful [9]. The curvature free energy G is expanded in the principal curvatures c_1 and c_2 [37],

$$G\left(c_1, c_2\right) = \int dA \left(\frac{\kappa}{2} \left(c_1 + c_2 - 2c_0\right)^2 + \bar{\kappa} c_1 c_2 \right), \tag{2.1}$$

where κ and $\bar{\kappa}$ are the elastic moduli and c_0 is the preferred curvature of the surface. c_0 is determined by the effective geometry of the surfactant as illustrated in Figure 2.2. The behaviour of microemulsions can now be fairly well explained in terms of these constants [7–9].

Chapter 3

Computer simulations

Fifty years ago, scientific research was either theoretical or experimental. These days, one often adds a third class: computational. This development is, of course, driven by the rapid development in computer technology. But parallel to this, theoretical models for the interaction between the building blocks of condensed matter (atoms and molecules) have improved and simulation techniques such as molecular dynamics and Monte Carlo were developed. These techniques provide a direct route between the microscopic and the macroscopic world, and constitute a link between theory and experiment. In fact, molecular simulations are virtual experiments on model systems. Depending on the complexity of the model, one can reach systems of the order 1–1000 nm and simulate for 1–1000 ns. The properties of matter at this scale differ substantially from the properties of single atoms as well as from what we observe in the macroscopic world.

3.1 Molecular simulations

The term molecular simulation covers numerical techniques that discretize matter into particles and simulate their evolution in accordance with a model for the inter-particle forces [38]. Molecular dynamics, Monte Carlo, and dissipative particle dynamics are examples that will be discussed below. In contrast, continuum models, field theories, and lattice models do not fall into this category.

The particular choice of technique depends mainly on the length and time scales of interest, but also on the quantities of interest (e.g. static or dynamic). For some problems, quantum effects must be taken into account. This requires ab initio simulations and implies solving the Schrödinger equation at every time step, which becomes computationally demanding for anything more than a few molecules. However, there are many applications in the condensed matter sciences where the precise electronic structure is unimportant. One can then approximate the atomic interactions with a classical potential.

In general, such a potential can be expressed as a sum of two-body, three-body,

etc contributions:

$$U\left(\mathbf{r}^N\right) = \sum_{\substack{i,j \\ i<j}} u_2\left(\mathbf{r}_i, \mathbf{r}_j\right) + \sum_{\substack{i,j,k \\ i<j<k}} u_3\left(\mathbf{r}_i, \mathbf{r}_j, \mathbf{r}_k\right) + \ldots \tag{3.1}$$

where $\mathbf{r}_i$ is the position of particle i and $\mathbf{r}^N \equiv \mathbf{r}_1, \mathbf{r}_2, \cdots, \mathbf{r}_N$. Often, pair-potentials suffice, e.g. to model van der Waals and electrostatic forces. For metals and semiconductors it is usually necessary to take into account a directional dependence, which requires three-body potentials. Molecules are often modelled with two-body, three-body, and four-body potentials that describe bond stretching, bond bending, and bond rotational energies, respectively, in addition to pair-wise non-bonded interactions.

With a classical inter-particle potential, Newton's second law (force equals mass times acceleration) gives the equations of motion for each particle i:

$$m_i \frac{d^2\mathbf{r}_i}{dt^2} = -\frac{\partial U\left(\mathbf{r}^N\right)}{\partial \mathbf{r}_i}, \tag{3.2}$$

where m_i is the mass of particle i. The molecular dynamics (MD) technique solves these equations numerically. Care must be taken to use an integration scheme and a time step that do not violate the energy conservation implicit in Newton's equations. A commonly used scheme is the Verlet algorithm [38].

Unless one is interested in certain molecules in vacuum or near walls, it is common to use periodic boundary conditions. This is a very effective way of avoiding wall-effects and thus effectively simulating an infinitely large system. Part of such a system is shown in Figure 3.1. The solid lines indicate the simulation box and the dashed lines indicate its periodic images. Particles near the walls interact with the periodic image of particles at the opposite side of the box. When a particle moves out of the box, its periodic image enters on the other side. The system must be large enough (compared to the range of the interactions) so that particles do not interact with their own periodic image.

MD is a dynamic technique that can be used to compute equilibrium quantities as well as transport properties. In contrast, Monte Carlo (MC) is a stochastic technique. While MD is based on Newton's equations, MC simulations generate configurations distributed according to the Boltzmann probability distribution:

$$P\left(U\left(\mathbf{r}^N\right)\right) = \frac{\exp\left(-\beta U\left(\mathbf{r}^N\right)\right)}{\int \mathbf{dr}^N \exp\left(-\beta U\left(\mathbf{r}^N\right)\right)}, \tag{3.3}$$

where $\beta \equiv k_B T$. The core operation in an MC simulation is to randomly generate trial moves, and accept or reject the moves according to acceptance rules. The acceptance rules ensure that the configurations satisfy the particular probability distribution.

Basic MD produces an NVE ensemble (microcanonical, with constant number of particles N, volume V, and energy E), while basic MC produces an NVT ensemble (canonical, constant temperature rather than energy). There are various ways

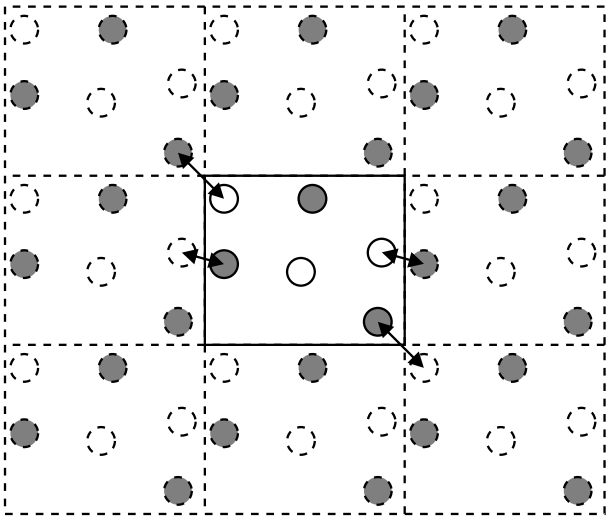

Figure 3.1: Schematic picture of a simulation box (solid boundaries) and its periodic images (dashed boundaries). The arrows indicate pair-wise forces.

of simulating other ensembles, for example a canonical ensemble with MD, or a constant pressure ensemble with MC. This will be reviewed in section 3.3.

A clear advantage of MD over MC is that it is dynamic. Nevertheless, the fact that one can perform unphysical moves with Monte Carlo is sometimes very useful. There are numerous practical reasons to sometimes prefer one method over the other. However, in the same ensemble, and in an infinitely long simulation, they do yield the same results. This is stated in the ergodicity theorem:

$$\bar{A} \equiv \lim_{t\to\infty} \frac{1}{t} \int_0^t A\left(\mathbf{r}^N\left(t'\right)\right) dt' = \int \mathbf{dr}^N A\left(\mathbf{r}^N\right) P\left(U\left(\mathbf{r}^N\right)\right) \equiv \langle A \rangle. \tag{3.4}$$

The time average of a given quantity, $\bar{A}$, equals the ensemble average $\langle A \rangle$ (under the same thermodynamic conditions). This means that evolving the system in time (MD) infinitely long, gives the same equilibrium quantities as sampling infinitely many independent configurations that have energies that follow the Boltzmann distribution (MC).

In many systems, e.g. emulsions, colloidal suspensions, and polymer solutions, the atomic details are not essential in order to model phase behaviour. Moreover, such detail prohibits reaching the time and length scales that are relevant in these systems. It is therefore common to apply coarse-grained models, i.e. lumping several atoms or molecules into one particle. Both MD and MC are equally suitable for coarse-grained interaction models as for atomistic models. However, there are alternative dynamic methods to MD which can speed up the simulation if one is willing to sacrifice atomic detail. Brownian dynamics and dissipative particle dynamics both incorporate frictional and fluctuating forces in addition to the conservative forces. The work described in this thesis was performed using dissipative particle dynamics.

3.2 Dissipative particle dynamics (DPD)

Dissipative particle dynamics (DPD) was introduced by Hoogerbrugge and Koelman as a new method to simulate microhydrodynamics [39]. The new technique features the best of two well established methods, MD and Lattice Gas Automata (LGA). On one hand, LGA and Lattice-Boltzmann methods suffer from a lack of isotropy and Brownian dynamics from a lack of momentum conservation, which is necessary to preserve hydrodynamics. On the other hand, MD stands on a firm theoretical basis, but is too detailed to access mesoscopic and hydrodynamic scales. With DPD, they arrived at a particle-based, mesoscopic simulation technique in which momentum is conserved.

Español and Warren made a significant contribution to the theoretical foundation of DPD when they linked DPD to a Fokker-Planck equation and showed that a canonical distribution can be obtained with a proper choice of dissipative and random forces [40]. With this link to statistical mechanics, DPD could be viewed simply as a mesoscopic MD technique in the NVT ensemble.

Originally aimed at microhydrodynamics, early applications of DPD include multiphase flow and colloidal dynamics [41]. Gradually it has become a popular technique to simulate complex fluids such as polymer solutions [42, 43], membranes [44–49], and surfactants [50–56]. The method is, however, still under development. There are several unresolved issues, the most prominent being how to define the mapping of time and length scales. Moreover, there are now several versions of the method which differ not only in the implementation, but also in the understanding of what the dissipative particles are.

3.2.1 DPD as coarse-grained MD

By using coarse-grained models, one effectively averages over some internal interactions. Addition of random and dissipative forces can mimic the effect of these lost degrees of freedom. The implementation of DPD in this work follows that of Groot and Warren [57]. In addition to conservative forces, pair-wise random and dissipative forces act between two particles i and j which are a distance r_{ij} apart. The equations of motion (Eq. 3.2) are modified to

$$m_i \frac{d^2\mathbf{r}_i}{dt^2} = -\frac{\partial U\left(\mathbf{r}^N\right)}{\partial \mathbf{r}_i} + \sum_j \left[\mathbf{F}_{ij}^R + \mathbf{F}_{ij}^D\right]. \tag{3.5}$$

The random and dissipative forces take the form

$$\mathbf{F}_{ij}^R = \sigma w^R\left(r_{ij}\right)\theta_{ij}\hat{\mathbf{r}}_{ij} \tag{3.6}$$

$$\mathbf{F}_{ij}^D = -\eta w^D\left(r_{ij}\right)\left(\hat{\mathbf{r}}_{ij}\cdot\mathbf{v}_{ij}\right)\hat{\mathbf{r}}_{ij}, \tag{3.7}$$

where $\mathbf{v}_{ij}$ is the velocity difference for the two particles and $\hat{\mathbf{r}}_{ij}$ is the unit vector pointing from particle j to particle i. θ_{ij} is a random number with Gaussian statistics [57], σ and η determine the amplitude of the random and dissipative forces,

respectively, and the w's are weight functions. The fluctuation-dissipation theorem requires $w^D = \left(w^R\right)^2$ [40]. The canonical temperature then follows from the relation between σ and η:

$$\sigma^2/\eta = 2k_BT. \tag{3.8}$$

The weight function $w(r) = w^R(r) = \sqrt{w^D(r)}$ can be chosen at will. The most common choice is simply:

$$w(r) = \begin{cases} 1 - \frac{r}{r_c} & \text{for} \quad r < r_c \\ 0 & \text{for} \quad r \geq r_c \end{cases} . \tag{3.9}$$

There seems to be no physical reason to apply a more sophisticated weight function, but it was recently shown that the discontinuous derivative is the source of numerical errors in commonly used integration schemes [58].

In principle, the dissipative and random forces can be applied in combination with any conservative force. In practice, two choices dominate in the literature: In polymer and colloidal solutions, the solvent is frequently modelled as an ideal, dissipative fluid, i.e. with $F^C = 0$. In surfactant and membrane applications, the non-bonded interactions are often

$$\mathbf{F}_{ij}^C = aw(r_{ij})\,\hat{\mathbf{r}}_{ij}, \tag{3.10}$$

where the amplitude a distinguishes different types of particles. This model will be discussed in detail in section 3.4.

The present combination of random and dissipative forces conserves momentum locally, which is necessary to produce the correct Navier-Stokes hydrodynamics. This requirement is not fulfilled by Brownian dynamics.

3.2.2 Drawbacks and alternative implementations of DPD

A serious drawback with this scheme is that the time scale is not very well defined. This is to some extent also true for the length scale. Resolving the length scale depends on realistic models for the effective forces between the lumps of atoms represented by dissipative particles. The time scale is trickier to map. For example, the amplitude of the dissipative force is clearly related to the viscosity, but the exact connection remains unclear and there is a discrepancy between predicted transport coefficients and theoretical benchmarks [59]. There were also attempts to deduce the time scale from self-diffusion coefficients [42, 44]. However, the concept of a diffusing DP bead is unclear, since the underlying atoms would not necessarily diffuse in the same direction.

Following attempts to resolve these issues, other implementations of DPD have appeared. Español et al developed a version of DPD with a fluid particle model that is thermodynamically more consistent [60, 61]. Their method differs more from MD in the sense that the particles are true thermodynamic subsystems and the model

parameters are thermodynamic properties and transport coefficients. They developed two methods, one based on the smoothed particle hydrodynamics method [61] and one using Voronoi fluid particles [60]. These formulations can also incorporate energy conservation, which makes it possible to study heat transport [62, 63].

3.2.3 Justification of the choice of method.

Most of this thesis focuses on equilibrium properties. Thus, no mapping of the time scales is required. The exception is paper V, which includes results on film rupture. This is a dynamic event, but also here, the emphasis is clearly on qualitative differences between surfactants and we make no attempt to quantify the time development. Thus, one might argue that molecular dynamics or Monte Carlo would be equally suitable for the present study. However, several practical reasons count in favour of DPD:

Phase space is in general more efficiently explored with a dynamic method (MD or DPD) than Monte Carlo. In particular, Monte Carlo moves of chain molecules is time consuming, and configurational-biased techniques are necessary [38, 53].

The combination of dissipative and random forces provides a built-in thermostat. For most applications, the canonical ensemble is clearly preferred to the microcanonical. The fluctuating forces also drive Brownian motion. This means that the system relaxes faster toward equilibrium. In the applications described in papers I–V, it means that micelles diffuse faster, and surface undulation modes develop faster than in the absence of these forces.

The simplicity of the conservative forces commonly employed with DPD is another advantage. (They are strictly speaking not part of the technique, but often associated with it.) The success of the Groot and Warren implementation of DPD is partly due to the fact that complex systems, for example binary mixtures, can be created easily and intuitively by adjusting the repulsion amplitude a between dissipative beads, and beads can readily be connected into surfactants and polymers. In contrast, Español et al create complex systems not by modifying the conservative forces, but with additional internal variables [64].

3.2.4 Integration algorithm

The most common, and usually the best, numerical scheme to integrate the equations of motion (Eq. 3.2) in MD is the (velocity) Verlet algorithm [38]:

$$\mathbf{r}_i(t+\Delta t) = \mathbf{r}_i(t) + \mathbf{v}_i(t)\,\Delta t + \frac{\mathbf{F}_i(t)}{2m_i}\Delta t^2 \tag{3.11}$$

$$\mathbf{v}_i(t+\Delta t) = \mathbf{v}_i(t) + \frac{\mathbf{F}_i(t+\Delta t) + \mathbf{F}_i(t)}{2m_i}\Delta t. \tag{3.12}$$

Here, $\mathbf{r}_i$ is the position, $\mathbf{v}_i$ is the velocity and $\mathbf{F}_i$ is the force for a particle i. This algorithm is time reversible and the error in $\mathbf{r}$ is of the order $(\Delta t)^4$ [38].

With only conservative forces, $\mathbf{F}(t+\Delta t)$ depends only on $\mathbf{r}(t+\Delta t)$. The problem with DPD in this respect is that the forces depend not only on the positions but also on the velocities. This means that the Verlet algorithm cannot simply be transferred to DPD [57]. In order to have time reversibility, $\mathbf{v}(t+\Delta t)$ and $\mathbf{F}(\mathbf{r}(t+\Delta t), \mathbf{v}(t+\Delta t))$ must be consistent [59]. This turned out to be nontrivial.

Temperature control and time reversibility were not considered in the original version of DPD, which made use of the Euler algorithm [39]. Groot and Warren [57] introduced a phenomenological tuning parameter λ to the Verlet scheme to mimic higher order schemes:

$$\mathbf{r}(t+\Delta t) = \mathbf{r}(t) + \mathbf{v}(t)\Delta t + \frac{\mathbf{F}(t)}{2m}\Delta t^2 \tag{3.13}$$

$$\tilde{\mathbf{v}}(t+\Delta t) = \mathbf{v}(t) + \lambda \mathbf{F}(t)\Delta t/m \tag{3.14}$$

$$\mathbf{F}(t+\Delta t) = \mathbf{F}(\mathbf{r}(t+\Delta t), \tilde{\mathbf{v}}(t+\Delta t)) \tag{3.15}$$

$$\mathbf{v}(t+\Delta t) = \mathbf{v}(t) + \frac{\mathbf{F}(t+\Delta t) + \mathbf{F}(t)}{2m}\Delta t. \tag{3.16}$$

The optimal value of λ for given densities and dissipation rates was determined from how well the temperature is conserved. At $\rho = 3$ and $\sigma = 3$, Groot and Warren recommended $\lambda = 0.65$. This combination was used in papers I–IV, with $\Delta t = 0.03$. This gave a temperature within 0.1% of the thermostat set point [56]. However, Hafskjold et al pointed out that the excellent temperature conservation is due to two errors that cancel at this particular combination of parameters [58]. This is also discussed in the appendix of paper V.

Several new integration schemes have been proposed, some based on self-consistent update of Eq. (3.12) by iteration [59, 65, 66]. In particular, the results for an ideal dissipative gas improve with multiple iterations. The drawback is increased CPU time. Lowe [67] avoided the problem of integrating the dissipative force by introducing a stochastic thermostat with similar properties. Recently, Shardlow [68] proposed an algorithm based on splitting the forces: The conservative part is solved using the Verlet scheme and the fluctuation/dissipation part is solved as a stochastic differential equation. This is also the basis of the Peters thermostat [69]. The Peters thermostat is described in the appendix of paper V along with the reasons for choosing this thermostat in paper V.

An argument made by both Hafskjold et al [58] and Peters [69] is that the large time steps frequently used in DPD cause errors in the integration of the conservative force. With the Peters thermostat, the errors in equilibrium properties are solely due to the conservative forces. With $\Delta t = 0.03$, the temperature deviation is 0.5% [56].

3.3 DPD in various ensembles

Newton's equations conserve energy. Therefore, a standard MD simulation produces a NVE ensemble. The simplest Monte Carlo scheme produces a NVT ensemble, with

temperature as specified in the Boltzmann factor in the acceptance rules. Also DPD gives an NVT ensemble, with temperature specified by the dissipative and random force amplitudes.

The NVE ensemble is rarely suitable in practice. It corresponds to a closed, isolated, rigid box – it cannot expand, and neither particles nor heat can be exchanged with the surroundings. To relate the simulation to experiments one would usually like to specify the pressure rather than the volume, and the temperature rather than the energy. Sometimes it is also useful to specify the chemical potential μ rather than the number of molecules, for example when studying phase equilibria: Two systems in equilibrium have the same temperature and pressure, but the density may differ. One does not know how many molecules are in either of the two phases, but the chemical potential is the same. Fortunately, there are ways to simulate NPT and μVT ensembles within the MD, DPD, and MC frameworks.

There are dynamic and stochastic ways of realizing other ensembles. The Nosé-Hoover and Anderson thermostats [38], commonly used to achieve NVT-MD, are examples of each of these two methods, respectively. The Nosé-Hoover thermostat employs an extended Lagrangian to build temperature conservation into the equations of motion. The Andersen thermostat mimics stochastic collisions with a heat bath at constant temperature: At random intervals, particles are given new velocities drawn from the Maxwell distribution at the specified temperature.

3.3.1 Hybrid MC-DPD

In this work we have used Monte Carlo moves (the stochastic route) to realize constant pressure [52, 53], constant normal pressure [52, 53], constant surface tension [54, 55], and constant chemical potential [52, 53, 56]. The scheme is thus a hybrid MC-DPD scheme. Realizing constant P rather than V, for example, is done as follows: During a series of DPD steps, the volume is fixed. At random intervals, the volume is varied and the change is accepted or rejected according to the rules (described below). Thus, different constant V shells are visited during a simulation, and they are distributed according to the Boltzmann distribution at constant P. With this scheme, the instantaneous value of P (as calculated from the virial) fluctuates, even in a 'constant NPT' simulation. By 'constant' P we here mean that the finite system is in contact with, or equilibrium with, an infinite system which has a constant, fixed pressure [38], and similarly for constant μ, $P_\perp$, and γ. To ensure such equilibrium, the system must follow the appropriate probability distributions. Below we discuss the probability distribution and Monte Carlo acceptance rule for each ensemble used in papers I–V. It is instructive to first explain particle displacement moves, which constitute the core of a conventional NVT–MC routine.

Eqs. (3.17–3.22) give the probability distribution in the NVT ensemble, the

procedure to generate trial moves, and the acceptance criterion:

$$\begin{aligned} P(U) &\propto \exp(-\beta U) && (3.17)\\ i &= \mathrm{int}(RAN \cdot N) + 1 && (3.18)\\ x_{i,n} &= x_{i,o} + \Delta r_{\max}(2RAN - 1) && (3.19)\\ y_{i,n} &= y_{i,o} + \Delta r_{\max}(2RAN - 1) && (3.20)\\ z_{i,n} &= z_{i,o} + \Delta r_{\max}(2RAN - 1) && (3.21)\\ \mathrm{acc}(o \to n) &= \min[1, \exp(-\beta(U_n - U_o))]. && (3.22) \end{aligned}$$

RAN is a uniformly distributed random number between 0 and 1. $\Delta r_{\max}$ is the maximum displacement, the choice for $\Delta r_{\max}$ affects only the efficiency of the program. o and n denote the old and new configuration, respectively. $U_n - U_o$ is thus the change in the total potential energy due to the displacement of one particle. Note that other trial moves and acceptance rules are possible, but the combination must satisfy detailed balance [38].

3.3.2 Constant pressure

In the NPT ensemble the probability distribution modifies to

$$\begin{aligned} P(V,U) &\propto \exp\left[-\beta\left(U + PV - N\beta^{-1}\ln V\right)\right] && (3.23)\\ V_n &= V_o + \Delta V_{\max}(2RAN - 1) && (3.24)\\ \mathrm{acc}(o \to n) &= \min[1, \exp(-\beta[U_n - U_o + P(V_n - V_o) && (3.25)\\ &\quad -N\beta^{-1}\ln(V_n/V_o)])], && (3.26) \end{aligned}$$

where V_n and V_o are the new and old box volume, respectively, and $\Delta V_{\max}$ is the maximum volume change. Constant pressure is used in papers I and II. It is applied in order to ensure equilibrium between two systems, the first containing a homogeneous bulk phase and the second containing an oil/water interface. Eqs. (3.23–3.26) apply in both cases, but the scaling of the box is different. In the bulk case, the pressure is isotropic and the box lengths are all scaled with the same factor:

$$L_n = L_o\left(\frac{V_n}{V_o}\right)^{\frac{1}{3}}. \qquad (3.27)$$

In the heterogeneous system, however, the pressure is not isotropic. Only the component normal to the interface is constant through the system. The tangential component in the vicinity of the interface depends on the interfacial structure, whereas the normal pressure is exerted by the surroundings. To mimic these conditions, we keep the box area (the dimensions parallel to the projected interface) constant, and vary the volume by scaling only the box length L_z:

$$L_{z,n} = L_{z,o}\left(\frac{V_n}{V_o}\right). \qquad (3.28)$$

The coordinates of all particles are scaled by the same factor as the box lengths in the respective direction. Therefore the potential energy for all particles must be taken into account as well in Eq. (3.26).

3.3.3 Constant interfacial tension

The interfacial tension is defined as the energy required to increase the interfacial area by one unit:

$$\gamma = \left(\frac{dG}{dA}\right)_{T,P}. \tag{3.29}$$

For a one-component system, for example the liquid/gas interface of water, this number is a constant (at a given point on the coexistence line). If surfactant is present, the tension depends also on the surface density of this component. The tension γ and surface area A are conjugate thermodynamic variables, just like P and V. It is therefore not surprising that one can simulate at constant tension in much the same way as constant pressure. But a constant NVγT ensemble is only meaningful when there is a film or membrane of an additional component present such that the tension depends on the surface density of this component. For example, for amphiphilic films or membranes, the tension depends on the number of amphiphiles per unit area. In the constant tension ensemble the volume of the box is kept constant, but the box shape is varied [46]:

$$\begin{aligned} P(A,U) &\propto \exp\left(-\beta\left[U-\gamma A\right]\right) && (3.30)\\ L_{x,n} &= L_{x,o}+\Delta L_{\max}\left(2RAN-1\right) && (3.31)\\ L_{y,n} &= L_{x,n} && (3.32)\\ L_{z,n} &= L_{z,o}A_o/A_n && (3.33)\\ \mathrm{acc}\left(o\rightarrow n\right) &= \min\left[1,\exp\left(-\beta\left(U_n-U_o-\gamma\left(A_n-A_o\right)\right)\right)\right]. && (3.34) \end{aligned}$$

Again, $U_n - U_o$ is the energy difference due to rescaling of all the coordinates.

This method has mainly been used to simulate lipid bilayers [47–49]. Biological membranes are not subject to external constraints, and will therefore adapt a tensionless state. Imposing $\gamma = 0$ with this scheme is therefore a neat way to simulate these systems. In papers III–IV we have employed this scheme to impose zero and finite tension for surfactant monolayers on oil/water interfaces, applicable to microemulsions.

3.3.4 Constant chemical potential

Constant chemical potential is frequently used to simulate phase equilibria [38]. One can, for example, simulate two coexisting phases in separate simulation boxes and avoid the presence of an interface. Or one might know the chemical potential

of a component in, for example, an ideal gas or ideal solution, and want to compute the adsorption in another phase.

The probability distribution of particle numbers in the grand canonical (μVT) ensemble is

$$P(N,U) \propto \frac{\exp(\beta\mu N)\, V^N}{\Lambda^{3N} N!} \exp(-\beta U), \tag{3.35}$$

$$\tag{3.36}$$

where Λ^{3N} is the kinetic contribution to the partition function. The acceptance rates for insertion and removal of a particle are

$$\mathrm{acc}(N \to N+1) = \min\left[1, \frac{V}{\Lambda^3 (N+1)} \exp\left\{-\beta\left(U_{N+1} - U_N - \mu\right)\right\}\right] \tag{3.37}$$

$$\mathrm{acc}(N \to N-1) = \min\left[1, \frac{\Lambda^3 N}{V} \exp\left\{-\beta\left(U_{N-1} - U_N + \mu\right)\right\}\right]. \tag{3.38}$$

Whether to remove or to add a particle is chosen at random. For removal, a particle is chosen at random and for insertion, a new position is chosen at random. Within the hybrid MC-DPD scheme, inserted particles must also be given a velocity, drawn randomly from the Maxwell distribution.

A constant chemical potential is imposed for the surfactants in papers I–II and for water in paper V. In paper V, this is done to ensure that the emulsion film is in equilibrium with an implicit bulk water reservoir, corresponding to the continuous emulsion phase. The objective is to measure the forces between the two interfaces, i.e. the normal pressure in the system, as a function of the film separation. In addition to μ_{water}, V, and T, N_{oil} and N_{surf} are also kept constant. In this case, N in Eqs. (3.35–3.38) is replaced by N_{water}.

In papers I–II we impose the same μ_{surf} in a heterogeneous system that contains an oil/water interface, and a homogeneous system containing bulk water. The purpose is to relate the surface adsorption and surface tension to the surfactant concentration in the bulk. In a one-component system, the chemical potential is a unique function of P and T. Hence, there is no such thing as a μPT ensemble. Even if one tries to impose corresponding μ and P with the schemes above, such a simulation will be a random walk in V and N, since no extensive variable is specified. However, in papers I–II we simulate constant $\mu_{\mathrm{surf}}, N_{\mathrm{water}}, N_{\mathrm{oil}}, P_\perp$, and T for a system with an oil/water interface, and constant $\mu_{\mathrm{surf}}, N_{\mathrm{water}}, P, T$ for a bulk water system. These systems are bound by the extensive quantity N_{water} (and N_{oil} in the heterogeneous case). The ensembles are therefore well-defined, at least at low chemical potentials. At very high chemical potentials, the surfactants may form a separate phase that is not bound by the amount of water present. Then V and N_{surf} grow without bounds, like in the one-component case.

Since the solubility of oil in bulk water is very low, oil was not considered in the homogeneous system. However, micelles may solubilise oil into their interiors. In order to facilitate this, μ_{oil} must also be imposed in both systems.

Although both V and N_{surf} are varied in the same simulation, N_{surf} is constant during volume trial moves and V is constant during particle insertions/removals. Eqs. (3.23–3.26) and (3.35–3.38) therefore remain the same, but with $N = N_{\text{surf}} + N_{\text{water}} + N_{\text{oil}}$ in Eqs. (3.23–3.26) and $N = N_{\text{surf}}$ in Eqs. (3.35–3.38).

3.3.5 Chain molecules

A surfactant molecule consists of several DPD particles connected by harmonic springs. Chain molecules require some special considerations compared to single beads.

The computational efficiency of any Monte Carlo scheme relies on a significant acceptance probability. For particle displacements, box volume, and box shape changes it is possible to tune the maximum changes, $\Delta r_{\max}$, $\Delta V_{\max}$, and $\Delta L_{\max}$, respectively, to obtain a desired acceptance rate. The optimal acceptance rate (i.e. for which phase space is sampled most efficiently) depends on the particular application but is usually 20–50% [38]. However, insertion and removal of chain molecules in relatively dense fluids have an acceptance probability smaller by several orders of magnitude. The probability of random insertion at an 'empty spot', large enough for a chain molecule, is prohibitively small. Similarly, the probability of finding a large molecule which can be removed without leaving a large void is equally small. The solution is to apply a bias that finds such voids and molecules. Configurational-biased Monte Carlo for chain molecules is explained in paper II.

When applying the constant pressure algorithm, one has two options: Either rescale all center-of-mass positions and keep the bond lengths unchanged, or rescale all monomer positions. With the first choice, N in the acceptance rules should be the total number of molecules. With the second choice, it should be the total number of monomers. There seems to be no reason to prefer one over the other.

3.4 Model

3.4.1 A coarse-grained model for amphiphiles

Surfactants consist of at least one hydrophilic and one hydrophobic part. Thus, the simplest surfactant model is a dumb-bell of two mutually immiscible beads [19]. In reality there are thousands of different surfactants – most consist of one or several hydrocarbon chains, while the hydrophilic part can take any 'shape' and 'size' [1]. An example of a simple, ionic surfactant is the sodium-dodecyl-sulfate (SDS) with chemical formula $CH_3(CH_2)_{11}SO_4^-Na^+$. In water, the sodium ion dissolves and the remaining part consists of an anionic, hydrophilic head group and a linear chain of alkyl groups. The polyoxyethylene alcohols, $C_nH_{2n+1}(OCH_2CH_2)_mOH$, constitute a group of non-ionic surfactants with various number of hydrophobic and hydrophilic units, n and m, respectively.

In order to simulate a particular surfactant, one should consider all-atom models. However, to study the effect of surfactants in general or general changes in structure, coarse-grained models are suitable. In this work we study systematically the effect of structural changes, such as varying n and m.

Bead-spring models of water-like and oil-like particles were first considered by Smit [19]. The beads were Lennard-Jones particles where the attractive part of the potential is reduced or removed between oil-like and water-like particles. Harmonic springs connected the beads into surfactants. This forms the basis also for the present model. Figure 1 in paper I shows some model surfactants and describes the nomenclature used throughout this thesis. Soft repulsive forces (Eq. 3.10) as well as dissipative and random forces act between all particles. However, the amplitude a can be tuned such that the repulsion is stronger between a hydrophilic and a hydrophobic bead than between two beads of the same type. We will now discuss the thermodynamic properties of this model.

3.4.2 The soft repulsive force model

There is evidence that coarse graining tends to soften the potential, and that effective forces are mainly repulsive [70]. Nevertheless, a rigorous method to derive coarse-grained potentials is still lacking. The present model (Eq. 3.10) is typically used to model soft matter [42–55]. Soft matter is condensed matter which is characterised by an energy scale close to the thermal energy and a length scale larger than the atomic length scale. Thus, entropy plays the predominant role. This is the reason why such a simple force model is sufficient to describe many aspects of such systems. The phase behaviour of, for example, biological membranes, polymer solutions and surfactant solutions depends on factors such as ordering, staggering, and available phase space for thermally vibrating chains.

A one-component system described by Eq. (3.10) has equation of state

$$P = \rho k_B T + 0.101 a \rho^2 \tag{3.39}$$

at $\rho > 3$ [57]. This model does not feature liquid-gas coexistence due to the absence of attractive forces. Liquid/liquid interfaces are, however, feasible. A two-phase, binary mixture can be created by choosing $a_{12} > (a_{11}, a_{22})$. Three parameters are in fact sufficient to create a simple oil/water/surfactant system, if a surfactant contains both type 1 and type 2 beads. A framework for deriving repulsion parameters from experimental data was published by Groot et al [42, 44, 57]. Diagonal elements a_{ii} are obtained by matching simulation results to bulk compressibilities, and off-diagonal elements a_{ij} can be related to Flory-Huggins χ-parameters. It is important to note that the values of these repulsion parameters are in general not independent of temperature and density.

3.4.3 Reduced units

In molecular simulations it is common to work with reduced units. This is particularly convenient if the models do not represent a particular compound, but are thought to apply to a general class of compounds. In DPD, a natural choice of units are the mass of a DPD bead m, the force cut-off distance r_c, and k_BT, where T is the temperature of the thermostat. All simulation results can be expressed as a combination of these units, e.g. time $t = r_c\,(m/k_BT)^{1/2}$ and surface tension $\gamma = k_BT/r_c^2$. To translate the simulation units into SI units, one must know the values m, r_c, and k_BT in SI units. With a DPD bead representing three water molecules, $r_c = 6.46$Å, $m = 8.98 \cdot 10^{-26}$kg, and $T = 298$K, a time step of 0.03 in reduced units represents $t = 0.03 \times r_c\,(m/k_BT)^{1/2} = 3.02 \cdot 10^{-12}$ seconds, and an interfacial tension of 3.45 translates to $\gamma = 3.45 \times k_BT/r_c^2 = 34.0$mN/m. We stress, however, that the model is too simple to expect quantitative agreement with experimental data in most of the cases. All conclusions drawn in this thesis are qualitative, and the results are therefore reported only in reduced units.

3.4.4 Parameter sets

A number of parameter sets for surfactants, polymers, and lipids in water exist in the literature [42, 44, 45, 50, 51, 57, 71]. It is common to define $k_BT = 1$ at room temperature and simulate at $\rho = 3 - 5$. The repulsion parameters depend on the desired level of coarse-graining. Early papers suggested $a_{\mathrm{ww}} = 25$ [42, 57], but according to Groot and Rabone [44],

$$a_{\mathrm{ww}} = 78N_m/\rho \tag{3.40}$$

for water at room temperature, where N_m is the number of water molecules mapped onto a dissipative particle. It seems that N_m should be at least 3–5 in order to justify "wiping out" the molecular details and the hard core repulsions. Nevertheless, $a_{\mathrm{ww}} = 25$ still dominates in the literature, or even lower at higher densities [51], along with surfactant models consisting of only one head and one tail, i.e. N_m closer to 10. This is the basis for parameter set A in Table 3.1.

Table 3.1: Repulsion parameters a_{ij}. w = water, o = oil, t = tail, and h=head. Set A is based on Groot [42] with o=t, but with $a_{\mathrm{oo}} = 25$ rather than 15 to obtain a symmetric oil/water model. Set B is from Groot and Rabone [44].

A	w	o/t	h
w	25	80	15
o/t	80	25	80
h	15	80	35

B	w	o/t	h
w	78	104	75.8
o/t	104	78	104
h	75.8	104	86.7

The effect of surfactant structure is the focus of the present study. The volume of a CH_2 group is roughly equal to the volume of a water molecule. $N_m = 3$ is therefore a desired level of detail. Based on Eq. (3.40), $a_{\mathrm{ww}} = 78$, and this is the basis for parameter set B in Table 3.1.

The phase-behaviour depends largely on the off-diagonal terms [71]. The oil-water miscibility is directly related to the a_{wo} parameter. The solubility of surfactants in bulk oil and water can be tuned by adjusting a_{oh} and a_{wt}. Groot chose $a_{\mathrm{hh}} > a_{\mathrm{tt}}$ to favour spherical micelles in water, and $a_{\mathrm{wh}} < a_{\mathrm{ww}}$ to model hydration of the head groups [42]. This is adopted in both parameter sets in Table 3.1.

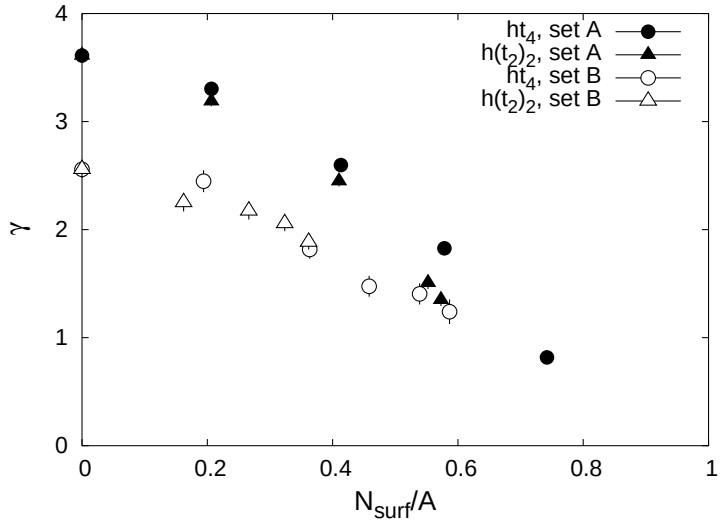

Figure 3.2: The interfacial tension as a function of the surface density of surfactant for ht_4 (linear) and $h(t_2)_2$ (branched) surfactants with parameter sets A and B. The models are drawn in Figure 1 in paper I.

Kranenburg et al undertook a detailed comparison of parameter set A and B and an all-atom model, concluding that the magnitude of a_{ww} had little influence and the difference $a_{\mathrm{wt}} - a_{\mathrm{ww}}$ had a significant influence on density profiles and phase behaviour of lipid membranes [71]. Figure 3.2 shows interfacial tension as a function of interfacial density of surfactant for linear and branched surfactants with each of the two parameter sets. A larger $a_{\mathrm{wt}} - a_{\mathrm{ww}}$ difference in A gives generally higher interfacial tension. The effect of surfactants is similar with the two sets; if we plot γ/γ_0, the results fall more or less on the same line (not shown). Figure 3.3 shows the distribution of head groups in the simulation box with 180 ht_4 surfactants in total. The main difference between the two sets is that set B gives lower interfacial adsorption and higher solubility in oil. On this basis we chose to proceed with set A. This set is used in the remaining part of this thesis. Figure 3.2 shows also that the difference between branched and linear surfactants disappear with set B. This was investigated in detail in papers I–II.

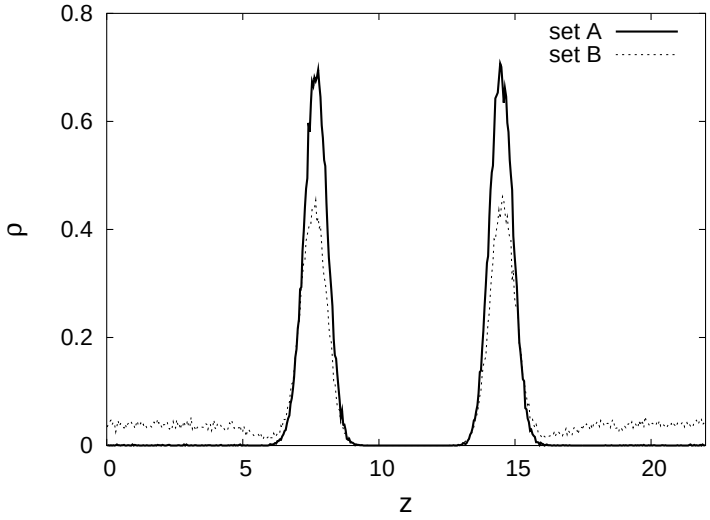

Figure 3.3: The density distribution of the head groups with the two parameter sets. The simulation box has dimensions $11 \times 11 \times 22$ and contains 180 ht_4 surfactants.

3.4.5 Bonded interactions

The simplest way to realize bonded interactions is with harmonic springs:

$$U^{\text{bond}}(r) = \frac{k_s}{2}(r - r_0)^2 \tag{3.41}$$

This model requires no constraints on the dynamics, and is thus significantly more convenient than fixed bond lengths. Furthermore, models that allow for chemical reactions are clearly unnecessary for this study. We chose $k_s = 100$ and $r_0 = 0.7$. The non-bonded interactions, Eq. (3.10), apply to all pairs including the bonded pairs. Figure 3.4 shows the bond length distribution in ht_4 surfactants at an oil/water interface.

3.4.6 Comparison with real surfactants

The quality of a model can only be evaluated by comparing a large range of simulation data to experimental data. A number of studies have shown that the DP models can indeed reproduce experimental phase diagrams of surfactant solutions [50, 51] and lipid bilayers [47–49].

In papers I–V we have used parameter set A, but in paper II we also study the effect of varying the surfactant parameters. The effects are quite intuitive, for example, lower head-head repulsion gives the same effect as obtained by adding salt to screen the ionic interactions with real surfactants. A lower oil-head repulsion gives a more oil-soluble head, causing surfactants to stagger at the interface. It is also clear that the somewhat unrealistically low solubility of surfactants in water is due to the high water-tail repulsion. Although a_{wt} is even higher in parameter set

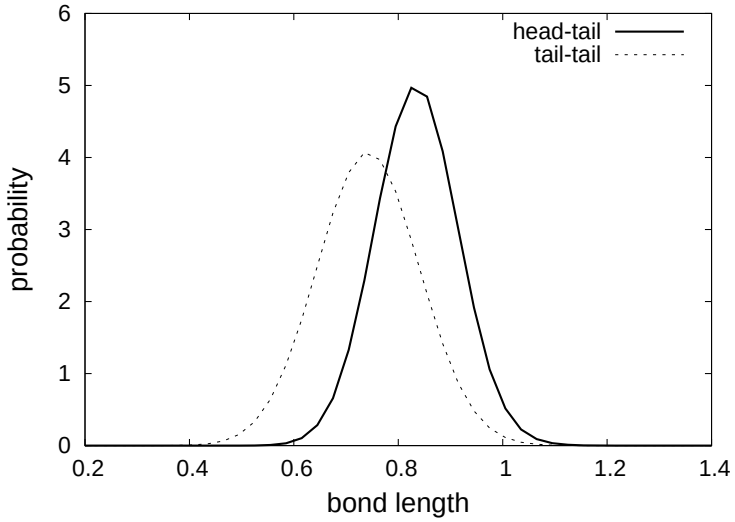

Figure 3.4: The distribution of bonds between head and tail groups (solid lines) and between two tail groups (dashed lines) for 180 ht_4 surfactants at the oil/water interface and box dimensions $11 \times 11 \times 22$.

B, the excess repulsion $a_{\mathrm{wt}} - a_{\mathrm{ww}}$ is lower, making both surfactants and oil more soluble in water with this set.

Groot chose a_{hh} and a_{hw} to resemble ionic surfactants that aggregate into spherical micelles (in the case of dumb-bell surfactants) [42]. However, it is clear that the model does not resemble long-range electrostatic interactions. This is evident in paper V, where long-range surface forces across an oil/water/oil film are absent. In this respect, the model should be thought of as a non-ionic surfactant with a relatively small head group (e.g. not a polyoxyethylene chain).

In contrast, the surfactant tails are very well described by the present model. This is because their effect is mainly entropic. An increase in surface tension (papers I–II) and bending rigidity (papers III–IV) with surfactant density and surfactant tail length is due to the constraints on available phase space for thermally vibrating tails. The surface forces in paper V originate in overlapping phase space for tails belonging to opposite interfaces.

Chapter 4

Fluid interfaces

Interpreting the results in papers I–V required a detailed study of the structure of oil/water/surfactant interfaces. In section 4.1 we present some typical density and pressure profiles that illustrate the general structure. In section 4.2 we discuss some choices and definitions that had to be made in order to pursue a quantitative description of the interface.

4.1 A microscopic view at the interface

4.1.1 The oil/water interface

Consider a heterogeneous system in which a liquid phase coexists with another liquid phase or a vapour. On a macroscopic scale, the interface is two-dimensional. Viewed on a microscopic scale, there is a region of finite thickness where the composition varies continuously. Figure 4.1 shows density profiles across an oil/water interface. It also shows the total density, which is lower in the interfacial region, due to the immiscibility of water and oil.

Gibbs defined the dividing surface as a surface in the mathematical sense, a geometric plane [72]. There are several ways to define such an interface. For a particular problem, one may be more practical than another. A common choice is the equimolar interface. The equimolar interface is defined with respect to one of the components, chosen as the reference component. Choosing oil as reference in Figure 4.1, the position of the equimolar surface $z_{\mathrm{em,o}}$ is defined by the equality

$$\int_0^{z_{\max}} \rho_{\mathrm{o}}(z)\, dz = z_{\mathrm{em}}\left(\rho_{\mathrm{o}}^{\mathrm{o}} - \rho_{\mathrm{o}}^{\mathrm{w}}\right) + z_{\max}\rho_{\mathrm{o}}^{\mathrm{w}} \tag{4.1}$$

where $\rho_{\mathrm{o}}(z)$ is the density of oil at position z and $\rho_{\mathrm{o}}^{\mathrm{o}}$ and $\rho_{\mathrm{o}}^{\mathrm{w}}$ are the densities of oil in bulk oil and bulk water, respectively. The position of $z_{\mathrm{em,o}}$ is indicated by arrows in Figure 4.1. Since the model is symmetric in oil and water and the simulation box contains an equal amount of both components, the equimolar surface for water is at $z_{\mathrm{em,w}} = z_{\max} - z_{\mathrm{em,o}}$, but $z_{\mathrm{em,o}}$ and $z_{\mathrm{em,w}}$ do not coincide.

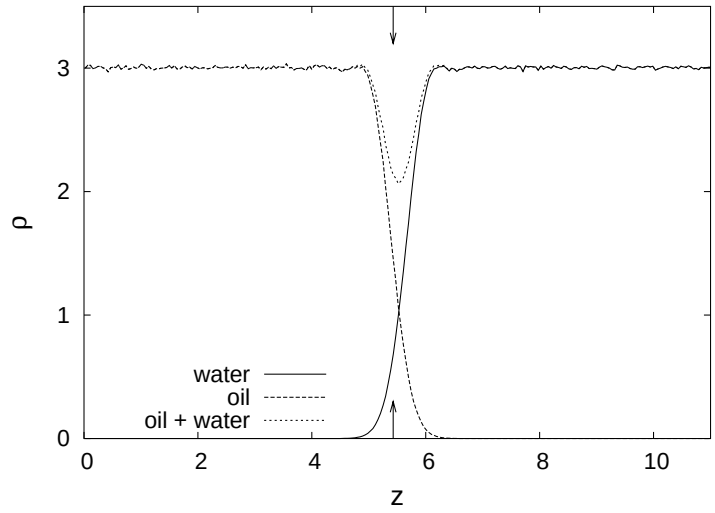

Figure 4.1: Density profiles for water and oil. The arrows indicate the position of Gibbs equimolar interface with respect to the oil phase.

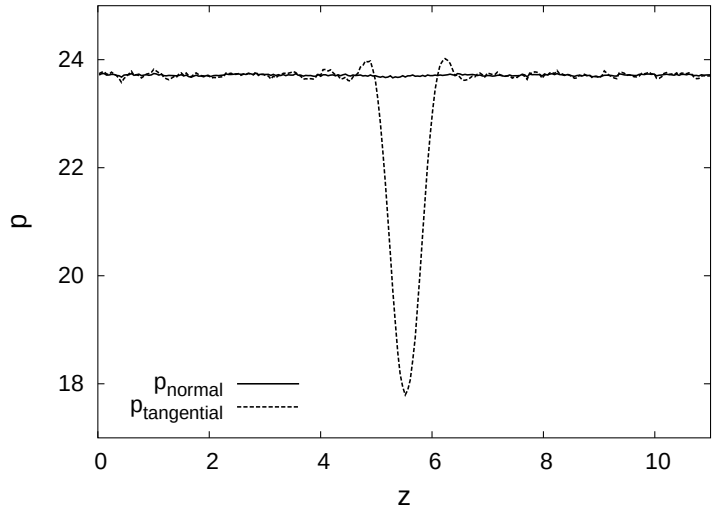

Figure 4.2: Normal and tangential pressure profiles in a system with oil and water.

Coarse-grained density and pressure profiles are computed by dividing the simulation box into slabs of thickness Δz parallel to the interface. The density of component a in slab number b is

$$\rho_a(z_b) = \frac{\langle N_a \rangle_b}{A\Delta z} \tag{4.2}$$

where $\langle N_a \rangle_b$ is the average number of particles of type a in slab b and A is the box area. Pressure profiles are computed according to the definitions of Irving and

Kirkwood [73, 74]. The pressure in slab b in direction α is

$$p_\alpha^b = \frac{\langle N \rangle_b}{A\Delta z} k_B T - \sum_{\substack{i,j \\ i<j}} \frac{F_{ij,\alpha} r_{ij,\alpha}}{A\Delta z} \times \phi\left(r_i, r_j, b\right) \tag{4.3}$$

where $r_{ij,\alpha}$ is the α-component of $\mathbf{r}_{ij}$ and $\phi\left(r_i, r_j, b\right)$ is the fraction of the straight line between i and j that lies within slab b.

The pressure profiles that correspond to the density profiles in Figure 4.1 are shown in Figure 4.2. Here, $p_\perp = p_z$ and $p_\parallel = \left(p_x + p_y\right)/2$. The normal pressure is constant through the interface, as required in mechanical equilibrium. The tangential pressure drops at the interface. The interfacial tension

$$\gamma = \int_0^{z_{\max}} \left[p_\perp\left(z\right) - p_\parallel\left(z\right)\right] dz \tag{4.4}$$

is a manifestation of the unfavourable interactions between oil and water molecules. These forces will result in a lower total density in the interfacial region, in order to maintain a constant normal pressure (Figure 4.1). Due to this lower density at the interface, the parallel pressure in this region is lower than in the bulk phases. The interface is thus under constant tension, attempting to minimise its area.

4.1.2 The effect of surfactants

Adsorption at the interface is defined as excess with respect to the chosen equimolar surface. The excess adsorption of surfactant is

$$\Gamma_{\text{surf}} = \int_0^{z_{\max}} \rho_{\text{surf}}\left(z\right) dz - \rho_{\text{surf}}^{\text{o}} z_{\text{em}} - \rho_{\text{surf}}^{\text{w}}\left(z_{\max} - z_{\text{em}}\right). \tag{4.5}$$

Figure 4.3 shows the density profiles with ht_4 surfactant present. The profile for each bead in the ht_4 surfactant is shown separately and shows that the distribution becomes wider the further away from the head group. This indicates that the tails are vibrating rather than stiff and straight. Since these surfactants are virtually insoluble in both bulk phases, the excess adsorption equals the number of surfactants per unit area.

The corresponding pressure profiles are shown in Figure 4.4. There is a pronounced change in the parallel pressure in the interfacial region compared to Figure 4.2. This explains why surfactants lower the interfacial tension: Interaction between surfactants, e.g. electrostatic repulsion between ionic head groups or excluded volume effects for thermally vibrating tails, increases the parallel pressure in the interfacial region. In Figure 4.4, the parallel pressure actually exceeds the normal pressure in the region of the tails.

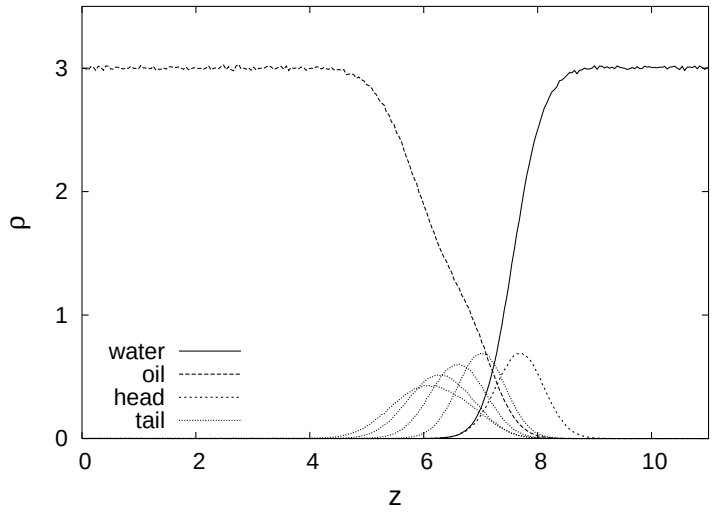

Figure 4.3: Density profiles for water, oil, and ht_4 surfactant.

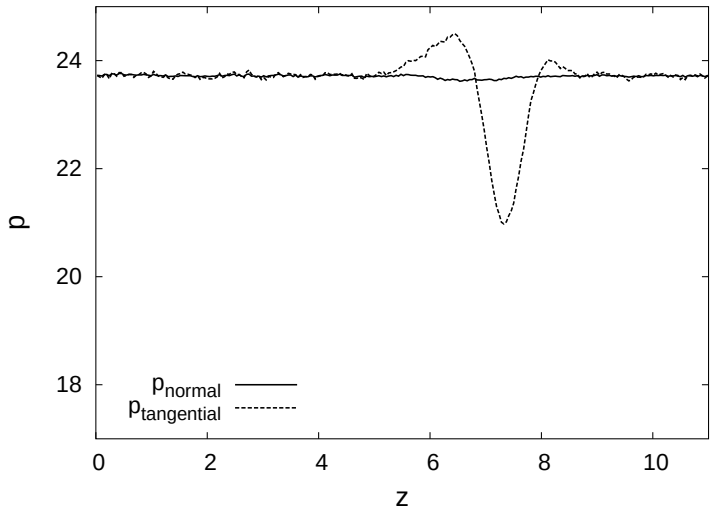

Figure 4.4: Normal and tangential pressure profiles in a system with water, oil, and ht_4 surfactant.

4.2 Characterising the interface

4.2.1 Surfactant adsorption

This thesis focuses on monolayers of surfactants adsorbed at oil/water interfaces. The aim is not as much to determine interfacial properties – that can be done more reliably in experiments – as to understand what molecular properties that cause these effects. To achieve an understanding of the molecular mechanisms, we need to know where the surfactants are, how they are arranged, etc. Such detailed infor-

mation about a system may explain why macroscopic properties respond to changes in structure in a certain way. This information is difficult to obtain experimentally, and this is where simulations can provide a significant contribution.

A quantity frequently encountered in the experimental literature is the area per surfactant, A_{surf}. Most results are therefore presented as a function of $N_{\text{surf}}/A \equiv A_{\text{surf}}^{-1}$ rather than the excess adsorption Γ_{surf}. There is also a practical reason for this choice: At high concentrations, the majority of surfactants in the bulk are in micelles. These are large and diffuse slowly. Computing the equilibrium bulk concentration accurately is therefore computationally very expensive.

Determining N_{surf}/A requires a definition of where the interface begins and ends, i.e. the integration limits a and b:

$$N_{\text{surf}}/A = \int_a^b \rho_{\text{head}}(z)\, dz \tag{4.6}$$

In practice, $\rho_{\text{head}}(z)$ is either negligible in the bulk (Figure 4.3) or exhibits a minimum between the interface and the bulk (Figure 3.3 and Figure 5c in paper II). We chose this minimum as the integration limit.

To characterise the undulation waves in papers III–IV, the instantaneous position of the interface is required. This means that surfactants must be assigned to the interface 'on the fly'. For this we used a cluster algorithm and a bond alignment criterion, described in detail in paper III.

4.2.2 Undulatory fluctuations

All interfaces considered here are flat on average. By 'flat on average' we mean the following: Due to the periodic boundary conditions (section 3.1), the condition

$$\lim_{x\to 0^+} f(x,y,z) \equiv \lim_{x\to L_x^-} f(x,y,z) \tag{4.7}$$

holds for any property f and any (y,z), and similarly in the two other directions. This implies that shape fluctuations in the interface can be expressed as a superposition of an integer number of waves, as opposed to vibrations on a string (1D) or drum (2D), which can be expressed as integers of half wave lengths. In other words, a region with negative curvature must coexist with a region with positive curvature.

This said, 'flat on average' is far from flat on a molecular scale. Thermal fluctuations induce undulation waves, and the density of such waves depends on the stiffness of the monolayer. Since such fluctuations also increase the total contact area between the immiscible phases, the wave density depends also on the interfacial tension.

The Helfrich model for the thermal fluctuations is described in paper III. This model defines the bending moduli κ and $\bar{\kappa}$. In papers III–IV the bending rigidity κ is computed from the fluctuation spectrum, which is the Fourier transform of

the instantaneous local height distribution $h(x, y, t)$. Unfortunately, there is no unambiguous way to define the surface $h(x, y, t)$.

A procedure to map beads (or other points in space) onto a two-dimensional grid is described in detail in paper III. The ambiguity lies in which bead(s) to consider in this mapping. We chose the head groups (the head group closest to the tails, in case of two heads). The computed undulation spectrum is thus, strictly speaking, the undulation wave spectrum for the head groups. The spectrum is only independent of the position in the molecular chain if the surfactants are arranged as depicted in Figure 4.5a. Here, the local density of any bead remains constant during the fluctuations. In contrast, if they arrange as in Figure 4.5b or c, there is only one surface at which the local bead density is uniform (at the heads in b and the last tail bead in c). This surface is defined as the surface of inextension [18]. Its position depends on the particular interactions, but it was assumed that it is close to the head beads [18].

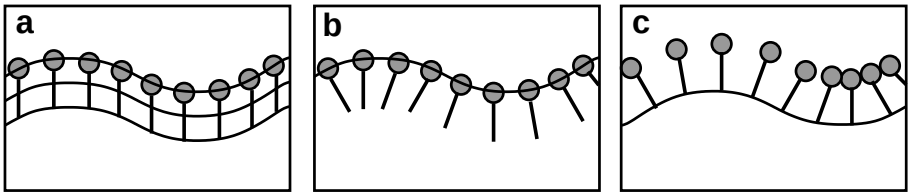

Figure 4.5: Some possible arrangements of surfactant during thermal undulations. The lines indicate surfaces of inextension, where the surface density of surfactant is constant during a fluctuation.

Figure 4.6 shows the spectrum for each bead in a ht_4 surfactant. The difference is small at low q (the undulation modes), but increases significantly for short wavelengths (the protrusion modes). There are several reasons for choosing the head group spectrum: First, this spectrum gives the best fit to the predicted spectrum. Second, it coincides with choices made in literature [18]. Third, the models under study employ no bond angle potentials, meaning that the tails are very flexible. Whereas the bond between the head and the first tail bead is expected to be aligned normally to the interface, this effect decreases for the consecutive tails, as can be seen in the bead density profiles in Figure 4.3. This means that there is much more disorder than in typical cartoon drawings like Figure 4.5. Such disorder may also account for the difference between the spectra in Figure 4.6.

4.2.3 Spontaneous versus average curvature

The spontaneous curvature c_0 of a monolayer is the curvature for which the first term of the Helfrich bending energy has a minimum (the second term is a topological constant). It is related to the geometry of the surfactant, but depends also on the external conditions, e.g. the density and the temperature. It is also closely related

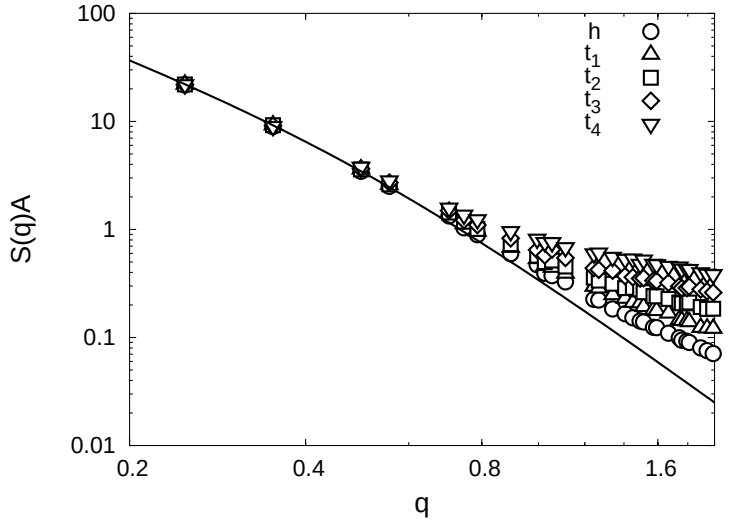

Figure 4.6: Fluctuation spectrum for each bead type in the ht_4 surfactant. The line is the best fit to $(\gamma q^2 + \kappa q^4)^{-1}$ where γ was measured independently and κ fitted to γ and the first 4 points in the head spectrum.

to the packing parameter discussed in section 2.1.1. Szleifer et al [18] derived an expression for c_0 in terms of the excess lateral pressure,

$$c_0 = \frac{1}{\kappa} \int_a^b \left[p_{\|}(z) - p_{\perp} \right] z dz, \tag{4.8}$$

with $z = 0$ at the surface of inextension, $z = a$ in bulk oil, and $z = b$ in bulk water. Based on Figure 4.4 one can conclude that $c_0 < 0$ for the ht_4 surfactant, even without knowing the precise position of the surface of inextension. This is the basis for the qualitative comparison with the channel nucleation theory for emulsion stability (paper V).

In all simulations with periodic boundary conditions, we have imposed an average curvature $\bar{c} = 0$. This is a realistic representation of macroemulsion droplets, but only an approximation for microemulsions and swollen micelles. It implies that, in papers III–IV, we have computed the spectrum for fluctuations away from the imposed average curvature $\bar{c} = 0$ instead of away from the spontaneous curvature c_0, which is nonzero except for symmetric surfactants.

Chapter 5

Conclusions and outlook

Papers I–V show that molecular simulations of coarse-grained surfactant models can improve our understanding of the behaviour of surfactants at oil/water interfaces. A systematic comparison of various model surfactants showed how structural changes affect interfacial properties. In general, the chain length and density dependence of the interfacial tension and bending modulus follow the experimental trends. However, a detailed look at the density and packing of surfactants revealed some interesting findings:

When comparing linear and branched surfactants at the same interfacial density, we found that branched surfactants can be either more or less efficient than their linear isomers, depending on the solubility of their head group in oil. If the head-oil repulsion is sufficiently low, the branched surfactants stagger and are therefore less efficient. Otherwise, the branched surfactants reduce the interfacial tension more than the linear ones. However, as the adsorption is higher for linear surfactants, they display a higher efficiency of adsorption also in the case where the head-oil repulsion is high enough to prevent staggering.

Another key result is the chain length dependence of the bending modulus. We confirmed a power-law dependence as previously found in experiments and computed by mean-field theory. However, we showed that the exponent depends on the conditions; it is lower at fixed zero tension, appropriate for microemulsions, than at fixed density as in the theoretical calculations.

The last paper shows that the presence of the non-ionic ht_4 and $h(t_2)_2$ model surfactants stabilise oil droplets in water and destabilise water droplets in oil. The fact that steric repulsive forces are observed only for approaching oil droplets is only part of the story. Even when forcing the droplets together, the oil/water/oil film ruptures earlier than the water/oil/water film. The problem is completely symmetric except for the surfactants, which have a negative spontaneous curvature. The difference between rupture of oil/water/oil films and water/oil/water films must therefore be related to the energy required to bend surfactants to create a channel between the drops. An expression for the channel free energy in terms of the spontaneous curvature and elastic constants was derived by Kabalnov and Wenner-

ström, showing that the spontaneous curvature largely influences the coalescence barrier [10]. The present simulations support their theory qualitatively, but in the future it would be interesting to compute the free energy of the channel between two oil and two water drops. This would enable a quantitative comparison of the coalescence barriers.

The results were obtained with a hybrid DPD-MC scheme. The coupling to various MC schemes was essential in order to mimic the experimental conditions, e.g. bulk-interface phase equilibria, microemulsions, and the surface force apparatus. DPD seems to be a good choice for this type of problems. Complex fluids call for a high degree of coarse graining and random forces to mimic the internal degrees of freedom. The conservative force models we have used are perhaps the simplest models that still enable systematic studies of structural variations. This was quite suitable for the present study, but it is clear that a good recipe for coarse graining molecules is needed in order to study specific compounds. Furthermore, some problematic aspects of the dynamics of DPD should clearly be addressed before using DPD to study surfactant dynamics.

Bibliography

[1] L. L. Schramm, E. N. Stasiuk, and D. G. Marangoni. Surfactants and their applications. *Annu. Rep. Prog. Chem., Sect. C*, 99:3–48, 2003.

[2] J. Sjöblom. *Emulsions and Emulsion Stability.* Dekker, New York, 1996.

[3] H. T. Davis. Factors determining emulsion type: hydrophile-lipophile balance and beyond. *Coll. Surf. A*, 91:9–24, 1994.

[4] D. N. Petsev, N. D. Denkov, and P. A. Kralchevsky. Flocculation of Deformable Emulsion Droplets. II. Interaction Energy. *J. Colloid Interface Sci.*, 176:201–213, 1995.

[5] J. N. Israelachvili. *Intermolecular and Surface Forces.* Academic Press, London, New York, 2th edition, 1991.

[6] J. N. Israelachvili and H. Wennerström. Entropic Forces between Amphiphilic Surfaces in Liquids. *J. Phys. Chem.*, 96:520–531, 1992.

[7] D. Langevin. Microemulsions - interfacial aspects. *Adv. Colloid Interface Sci.*, 34:583–595, 1991.

[8] M. Gradzielski. Bending constants of surfactant layers. *Curr. Opin. Colloid Interface Sci.*, 3:478–484, 1998.

[9] H. Wennerström, O. Söderman, U. Olsson, and B. Lindman. Macroemulsions versus microemulsions. *Coll. Surf. A*, 123–124:13–26, 1997.

[10] A. Kabalnov and H. Wennerström. Macroemulsion Stability: The Oriented Wedge Theory Revisited. *Langmuir*, 12:276–292, 1996.

[11] A. W. Adamson. *Physical Chemistry of Surfaces.* Wiley, 5th edition, 1990.

[12] H. M. Princen. The equilibrium shape of interfaces, drops, and bubbles. Rigid and deformable particles at interfaces. In E. Matijevic, editor, *Surface and Colloid Science.* Wiley-Interscience, 1969.

[13] J. Daillant and M. Alba. High-resolution x-ray scattering measurements: I. Surfaces. *Reports on progress in physics*, 63:1725–1777, 2000.

[14] J. R. Lu, R. K. Thomas, and J. Penfold. Surfactant layers at the air/water interface: structure and composition. *Adv. Colloid Interface Sci.* , 84:143–304, 2000.

[15] M. Gradzielski, D. Langevin, and B. Farago. Experimental investigation of the structure of nonionic microemulsions and their relation to the bending elasticity of the amphiphilic film. *Phys. Rev. E*, 53:3900–3919, 1996.

[16] I. Szleifer, D. Kramer, A. Ben-Shaul, D. Roux, and W. M. Gelbart. Curvature Elasticity of Pure and Mixed Surfactant Films. *Phys. Rev. Lett.*, 60:1966–1969, 1988.

[17] I. Szleifer, A. Ben-Shaul, and W. M. Gelbart. Chain Packing Statistics and Thermodynamics of Amphiphile Monolayers. *J. Phys. Chem.*, 94:5081–5089, 1990.

[18] I. Szleifer, D. Kramer, A. Ben-Shaul, W. M. Gelbart, and S. A. Safran. Molecular theory of curvature elasticity in surfactant films. *J. Chem. Phys.*, 92:6800–6817, 1990.

[19] B. Smit. Molecular dynamics simulations of amphiphilic molecules at a liquid-liquid interface. *Phys. Rev. A*, 37:3431–3433, 1988.

[20] B. Smit, P. A. J. Hilbers, K. Esselink, L. A. M. Rupert, N. M. van Os, and A. G. Schlijper. Computer simulations of a water/oil interface in the presence of micelles. *Nature*, 348:624–625, 1990.

[21] B. Smit, A. G. Schlijper, L. A. M. Rupert, and N. M. van Os. Effects of chain length of surfactants on the interfacial tension: Molecular dynamics simulations and experiments. *J. Phys. Chem.*, 94:6933–6935, 1990.

[22] N. M. van Os, L. A. M. Rupert, B. Smit, P. A. J. Hilbers, K. Esselink, M. R. Böhmer, and L. K. Koopal. Surfactant adsorption at liquid/liquid interfaces: comparison of experimental results with scf calculations and molecular dynamics simulations. *Coll. Surf. A*, 81:217–229, 1993.

[23] K. J. Klopfer and T. K. Vanderlick. Amphiphiles at oil-water interfaces: simulation study of their tension-reducing properties. *Coll. Surf. A*, 96:171–179, 1995.

[24] M. Laradji and O. G. Mouritsen. Elastic properties of surfactant monolayers at liquid-liquid interfaces: A molecular dynamics study. *J. Chem. Phys.*, 112:8621–8630, 2000.

[25] B. Smit, K. Esselink, P. A. J. Hilbers, N. M. van Os, L. A. M. Rupert, and I. Szleifer. Computer simulations of surfactant self-assembly. *Langmuir*, 9:9–11, 1993.

[26] S. Karaborni, K. Esselink, P. A. J. Hilbers, B. Smit, J. Karthäuser, N. M. van Os, and R. Zana. Simulating the Self-Assembly of Gemini (Dimeric) Surfactants. *Science*, 265:254–256, 1994.

[27] S. J. Marrink, D. P. Tieleman, and A. E. Mark. Molecular Dynamics Simulation of the Kinetics of Spontaneous Micelle Formation. *J. Phys. Chem. B*, 104:12165–12173, 2000.

[28] S. Karaborni, N. M. van Os, K. Esselink, and P. A. J. Hilbers. Molecular Dynamics Simulations of Oil Solubilization in Surfactant Solutions. *Langmuir*, 9:1175–1178, 1993.

[29] M. J. Rosen. *Surfactants and interfacial phenomena.* Wiley, New York, 2nd edition, 1989.

[30] J. N. Israelachvili. The science and applications of emulsions – an overview. *Coll. Surf. A*, 91:1–8, 1994.

[31] B. Widom, P. Bhimalapuram, and K. Koga. The hydrophobic effect. *Phys. Chem. Chem. Phys.*, 5:3085–3093, 2003.

[32] L. R. Pratt. Molecular theory of hydrophobic effects. *Ann. Rev. Phys. Chem.*, 53:409–436, 2002.

[33] G. Graziano. Comment on "The hydrophobic effect". *Phys. Chem. Chem. Phys.*, 6:4527–4528, 2004.

[34] M. J. Rosen. Geminis: A new generation of surfactants. *ChemTech*, March:30–33, 1993.

[35] M. Chappat. Some applications of emulsions. *Coll. Surf. A*, 91:57–77, 1994.

[36] J. Sjöblom, R. Lindberg, and S. E. Friberg. Microemulsions - Phase equilibria characterization, structures, applications and chemical reactions. *Adv. Colloid Interface Sci.*, 65:125–287, 1996.

[37] W. Helfrich. Elastic Properties of Lipid Bilayers: Theory and Possible Experiments. *Z. Naturforsch.*, 28c:693–703, 1973.

[38] D. Frenkel and B. Smit. *Understanding Molecular Simulations: from Algorithms to Applications.* Academic Press, San Diego, 2nd edition, 2002.

[39] P. J. Hoogerbrugge and J. M. V. A. Koelman. Simulating microscopic hydrodynamics phenomena with dissipative particle dynamics. *Europhys. Lett.*, 19:155–160, 1992.

[40] P. Español and P. B. Warren. Statistical mechanics of dissipative particle dynamics. *Europhys. Lett.*, 30:191–196, 1995.

[41] P. B. Warren. Dissipative particle dynamics. *Curr. Opin. Colloid Interface Sci.*, 3:620–624, 1998.

[42] R. D. Groot. Mesoscopic Simulation of Polymer-Surfactant Aggretgation. *Langmuir*, 16:7493–7502, 2000.

[43] F. Goujon, P. Malfreyt, and D. J. Tildesley. Dissipative Particle Dynamics Simulations in the Grand Canonical Ensemble: Applications to Polymer Brushes. *ChemPhysChem*, 5:457–464, 2004.

[44] R. D. Groot and K. Rabone. Mesoscopic Simulation of Cell Membrane Damage, Morphology Change and Rupture by Nonionic Surfactants. *Biophys. J.*, 81:725–736, 2001.

[45] J. C. Shillcock and R. Lipowsky. Equilibrium structure and lateral stress distribution of amphiphilic bilayers from dissipative particle dynamics simulations. *J. Phys. Chem.*, 117:5048–5061, 2002.

[46] M. Venturoli and B. Smit. Simulating the self-assembly of model membranes. *Phys. Chem. Comm.*, 10, 1999.

[47] M. Kranenburg, M. Venturoli, and B. Smit. Molecular simulations of mesoscopic bilayer phases. *Phys. Rev. E*, 67:060901, 2003.

[48] M. Kranenburg, M. Venturoli, and B. Smit. Phase Behavior and Induced Interdigitation in Bilayers Studied with Disipative Particle Dynamics. *J. Phys. Chem. B*, 107:11491–11501, 2003.

[49] M. Kranenburg and B. Smit. Simulating the effect of alcohol on the structure of a membrane. *FEBS Letters*, 568:15–18, 2004.

[50] P. Prinsen, P. B. Warren, and M. A. J. Michels. Mesoscale Simulations of Surfactant Dissolution and Mesophase Formation. *Phys. Rev. Lett.*, 89:148302, 2002.

[51] E. Ryjkina, H. Kuhn, H. Rehage, F. Müller, and J. Peggau. Molecular dynamic computer simulations of phase behavior of non-ionic surfactants. *Angew. Chem. Int. Ed.*, 41:983–986, 2002.

[52] L. Rekvig, M. Kranenburg, B. Hafskjold, and B. Smit. Effect of surfactant structure on interfacial properties. *Europhys. Lett.*, 63:902–907, 2003.

[53] L. Rekvig, M. Kranenburg, J. Vreede, B. Hafskjold, and B. Smit. Investigation of Surfactant Efficiency Using Dissipative Particle Dynamics. *Langmuir*, 19:8195–8205, 2003.

[54] L. Rekvig, B. Hafskjold, and B. Smit. Simulating the effect of surfactant structure on bending moduli of monolayers. *J. Chem. Phys.*, 120:4897–4905, 2004.

[55] L. Rekvig, B. Hafskjold, and B. Smit. Chain Length Dependencies of the Bending Modulus of Surfactant Monolayers. *Phys. Rev. Lett.*, 92:116101, 2004.

[56] L. Rekvig, B. Hafskjold, and B. Smit. Molecular simulations of surface forces and film rupture in oil/water/surfactant systems. *Langmuir*, in press.

[57] R. D. Groot and P. B. Warren. Dissipative particle dynamics: bridging the gap between atomistic and mesoscopic simulation. *J. Chem. Phys.*, 107:4423–4435, 1997.

[58] B. Hafskjold, C. C. Liew, and W. Shinoda. Can such Long Time Steps Really be used in Dissipative Particle Dynamics Simulations? *Mol. Sim.*, in press.

[59] I. Pagonabarraga, M. H. J. Hagen, and D. Frenkel. Self-consistent dissipative particle dynamics. *Europhys. Lett.*, 42:377–382, 1998.

[60] M. Serrano and P. Español. Thermodynamically consistent mesoscopic fluid particle model. *Phys. Rev. E*, 64:046115, 2001.

[61] P. Español and M. Revenga. Smoothed dissipative particle dynamics. *Phys. Rev. E*, 67:026705, 2003.

[62] P. Español. Dissipative particle dynamics with energy conservation. *Europhys. Lett.*, 40:631–636, 1997.

[63] J. B. Avalos and A. D. Mackie. Dissipative particle dynamics with energy conservation. *Europhys. Lett.*, 40:141–146, 1997.

[64] P. Español and C. Thieulot. Microscopic derivation of hydrodynamic equations for phase-separating fluid mixtures. *J. Chem. Phys.*, 118:9101–9127, 2003.

[65] G. Besold, I. Vattulainen, M. Karttunen, and J. M. Polson. Towards better integrators for dissipative particle dynamics simulations. *Phys. Rev. E*, 62:R7611–R7614, 2000.

[66] I. Vattulainen, M. Karttunen, G. Besold, and J. M. Polson. Integration schemes for dissipative particle dynamics simulations: From softly interacting systems towards hybrid models. *J. Chem. Phys.*, 116:3967–3979, 2002.

[67] C. Lowe. An alternative approach to dissipative particle dynamics. *Europhys. Lett.*, 47:145–151, 1999.

[68] T. Shardlow. Splitting for dissipative particle dynamics. *SIAM J. Sci. Comput.*, 24:1267–1282, 2003.

[69] E. A. J. F. Peters. Elimination of time-step effects in DPD. *Europhys. Lett.*, 66:311–317, 2004.

[70] B. M. Forrest and U. W. Suter. Accelerated equilibration of polymer melts by time-coarse-graining. *J. Chem. Phys.*, 102:7256–7266, 1995.

[71] M. Kranenburg, J.-P. Nicolas, and B. Smit. Comparison of mesoscopic phospholipid-water models. *Phys. Chem. Chem. Phys.*, 6:4142–4151, 2004.

[72] J. W. Gibbs. *The Scientific Papers of J. W. Gibbs*, volume 1. Dover, New York, 1961.

[73] J. H. Irving and J. G. Kirkwood. The statistical mechanical theory of transport processes. IV. The equations of hydrodynamics. *J. Chem. Phys.*, 18:817–829, 1950.

[74] T. Ikeshoji, B. Hafskjold, and H. Furuholt. Molecular-level Calculation Scheme for Pressue in Inhomogeneous Systems of Flat and Spherical Layers. *Mol. Sim.*, 29:101–109, 2003.

Collection of papers

I. Effect of surfactant structure on interfacial properties.
L. Rekvig, M. Kranenburg, B. Hafskjold, and B. Smit.
Europhys. Lett., 63:902–907, 2003.

II. Investigation of surfactant efficiency using dissipative particle dynamics.
L. Rekvig, M. Kranenburg, J. Vreede, B. Hafskjold, and B. Smit.
Langmuir, 19:8195–8205, 2003.

III. Simulating the effect of surfactant structure on bending moduli of monolayers.
L. Rekvig, B. Hafskjold, and B. Smit.
J. Chem. Phys., 120:4897–4905, 2004.

IV. Chain length dependencies of the bending modulus of surfactant monolayers.
L. Rekvig, B. Hafskjold, and B. Smit.
Phys. Rev. Lett., 92:116101, 2004.

V. Molecular simulations of surface forces and film rupture in oil/water/surfactant systems.
L. Rekvig, B. Hafskjold, and B. Smit.
Accepted for publication in *Langmuir*.

Paper I

EUROPHYSICS LETTERS 15 September 2003

Europhys. Lett., **63** (6), pp. 902–907 (2003)

Effect of surfactant structure on interfacial properties

L. Rekvig[1](*), M. Kranenburg[2], B. Hafskjold[1] and B. Smit[2]

[1] *Department of Chemistry, Norwegian University of Science and Technology N-7491 Trondheim, Norway*

[2] *Department of Chemical Engineering, University of Amsterdam Nieuwe Achtergracht 166, 1018 WV Amsterdam, The Netherlands*

(received 15 April 2003; accepted in final form 11 July 2003)

PACS. 82.70.Uv – Surfactants, micellar solutions, vesicles, lamellae, amphiphilic systems (hydrophilic and hydrophobic interactions).

PACS. 68.05.-n – Liquid-liquid interfaces.

Abstract. – We study surfactants at the oil/water interface using Dissipative Particle Dynamics simulations at constant $\mu_{\text{surf}}PT$. The interfacial tension depends on the surfactant branching in a subtle way. For a given interfacial concentration, a double-tail surfactant is more efficient than its single-tail isomer only if the oil-head repulsion is sufficiently strong. For a given concentration in the bulk water phase, the single-tail surfactants are more efficient in both cases. We interpret these results in light of the molecular packing at the interface and free-energy considerations.

Introduction. – Surfactants are molecules that consist of hydrophobic and hydrophilic parts. Their amphiphilic nature makes them surface active and, adsorbed at the oil/water interface, they can reduce the bare oil-water interfacial tension to very low values. Because of this property, surfactants are used in many practical applications ranging from crude oil recovery to state-of-the-art drug delivery [1] and are also of scientific interest. From a practical viewpoint, it is important to understand how the efficiency in reducing the interfacial tension is related to the structure of a surfactant. This question was already posed by Traube in 1899 [2] and he discovered that increasing the hydrophobic tail length results in surfactants that are more efficient (Traube's rule). At present, the effect of branching of the hydrophobic tail is not yet fully understood, despite the fact that many of the surfactants used in industrial applications are prepared with branched hydrocarbon tails. The effect of branching on the interfacial tension was investigated by self-consistent field calculations [3] and molecular-dynamics simulations on model surfactants [3, 4]. These studies agree on the fact that surfactants with two hydrophobic chains are less efficient in reducing the interfacial tension compared to their single-tail isomers. Experimentally, however, either more, equal, or less efficient branched surfactants are reported, depending on the details of the experimental setup [3, 5–8].

(*) On leave at Department of Chemical Engineering, University of Amsterdam, Amsterdam, The Netherlands. E-mail: live.rekvig@phys.chem.ntnu.no

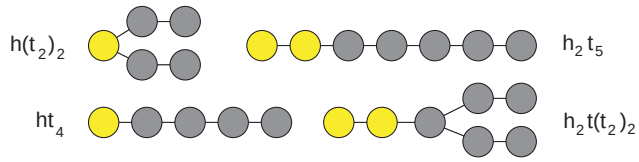

Fig. 1 – Some of the model surfactants and their respective names. Hydrophilic head beads (h) are shown in yellow and hydrophobic tail beads (t) are shown in gray.

Although it is assumed that branched molecules pack differently at the interface compared to linear ones [9,10], a molecular description of their tension-reducing properties is, to the best of our knowledge, still missing. In this work, we use Dissipative Particle Dynamics [11] (DPD) simulations to study the effect of branching on the interfacial properties of surfactants. Our simulations demonstrate that the head group properties determine the effect of branching on the interfacial tension, and we explain this by means of packing and ordering of the molecules at the interface. Furthermore, the efficiency also depends on the partitioning of the surfactant between the bulk liquid and the interface. Molecular simulation of a system with an interface in contact with its bulk phases cannot be used to effectively determine the bulk surfactant concentration due to the very low concentrations and long diffusion times involved. Here we present a method to overcome this problem, and report simulation results of interfacial tension *vs.* surfactant concentration in the bulk for both single-tail and double-tail surfactant structures.

Method and model. – In a DPD simulation one uses dissipative and random forces in addition to the conservative forces between the particles. The dissipative and random forces are chosen such that a proper Boltzmann distribution of configurations is sampled corresponding to the intermolecular interactions from which the conservative forces are derived [12]. In analogy with previous simulations of surfactants using the DPD technique [13], we use soft-repulsive interactions to mimic the mesoscopic interactions between the oil, water, and surfactant molecules. In our model, we distinguish four types of particles, o, w, h, and t, to mimic the oil, water, and the head and tail molecular groups of a surfactant, respectively. For the conservative forces we use the conventional soft repulsive interactions $F(r) = a(1 - r/r_{\mathrm{cut}})$ in which the parameters a are chosen such as to mimic the hydrophobic and hydrophilic interactions: $a_{\mathrm{ww}} = a_{\mathrm{oo}} = 25$, $a_{\mathrm{hh}} = 35$, $a_{\mathrm{wo}} = a_{\mathrm{oh}} = 80$, $a_{\mathrm{wh}} = 15$. The tail particles are identical to the oil particles. Our parameters are similar to those optimized by Groot [14], and reproduce the compressibility of water and solubility of non-ionic surfactant segments. The surfactant particles are connected via harmonic springs, with spring constant $k = 100$ and equilibrium distance $r_0 = 0.7$. Some of the surfactants models are pictured in fig. 1. This model maps typically 3-6 CH_2 groups onto one tail bead [13–15]. We simulated a system with approximately 8000 particles at temperature $T = 1.0$ and pressure $P = 23.6$ corresponding to a bulk density of 3.0. The box area was 11×11 and doubling the system size did not alter the results. All properties are expressed in the usual reduced units, *i.e.* using r_{cut}, repulsion parameter $a = 1$, and the mass of a DPD bead as units of length, energy, and mass, respectively. The interfacial tension was calculated by integrating the difference in normal and tangential pressure [16].

In previous simulations the interfacial tension was studied as a function of the total number of surfactants added to the system [3,4,16,17], whereas experimentally one usually determines the concentration of surfactants in the bulk phase. To determine the interfacial tension in a simulation one simulates the oil/water interface explicitly. In such an inhomogeneous system it is difficult to determine the concentration of the surfactants accurately. One not only needs relatively large systems to minimize the influence of the interface, but also very long

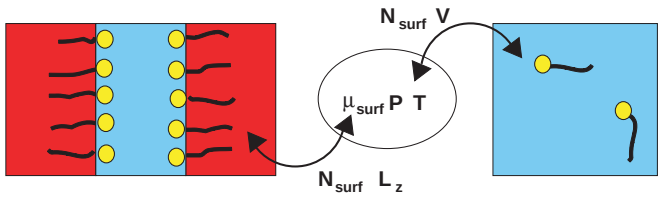

Fig. 2 – Simulation setup; the left figure is the inhomogeneous system that contains an oil/water interface and surfactants and the right figure is the homogeneous system containing water and surfactants. Both systems are coupled to a reservoir, which imposes the temperature, (normal) pressure, and chemical potential of the surfactants.

simulations since the concentration of surfactants in the bulk phase is usually very low. To determine the interfacial tension as a function of the surfactant concentration in the bulk, we introduce an ensemble in which we impose the temperature, (normal) pressure, and the chemical potential of the surfactant (μ_{surf}), see fig. 2. In this ensemble two systems are simulated; an inhomogeneous system containing the oil/water interface and a homogeneous system that contains the bulk water phase. The conventional DPD simulations, performed at constant number of particles (N), volume (V), and temperature, are combined with Monte Carlo moves in which we attempt to change the number of surfactant particles and a move in which we change the volume. For the inhomogeneous system we change the volume in such a way that the area of the oil/water interface remains constant, *i.e.* imposing the normal pressure. For a pure component one cannot impose both the chemical potential and the pressure, the extensive variables N and V would be unbounded [12]. In our system we keep the number of water (and oil) particles constant, hence fixing at least one extensive variable.

Similar to grand-canonical ensemble simulations, our ensemble relies on the successful insertion/deletion of the particles in the system. For atoms or small molecules this can be achieved by random insertion of the particles. For chain molecules, however, random insertion is very inefficient. To make this type of insertion moves possible for the surfactant molecules, we use the configurational-bias Monte Carlo technique [18] (CBMC). In a CBMC simulation a molecule is grown atom by atom in such a way that the "empty" spaces in the system are found. The bias introduced by this growing algorithm is removed exactly by adjusting the acceptance rules. With this CBMC scheme we obtain a sufficient number of accepted insertion and deletions in the inhomogeneous system to determine the interfacial concentration and tension. For our surfactant models, the concentrations in bulk water were found to be sufficiently low for Henry's law to be valid:

$$\frac{N_{\mathrm{surf}}}{V} = K_{\mathrm{H}} P_{\mathrm{surf}}. \tag{1}$$

Here K_{H} is the Henry coefficient and P_{surf} is the effective partial pressure of the surfactants in the reservoir. P_{surf} is directly related to μ_{surf}, which is imposed in the inhomogeneous system. K_{H} is related to the excess chemical potential at infinite dilution:

$$K_{\mathrm{H}} = \beta \exp\left[-\beta \mu_{\mathrm{surf}}^{\mathrm{excess}}\right]. \tag{2}$$

$\mu_{\mathrm{surf}}^{\mathrm{excess}}$ can be computed using a test particle method based on the CBMC scheme [12].

Interfacial tension vs. interfacial density. – Figure 3a) shows the interfacial tension as a function of surfactant concentration at the interface for various surfactant structures. At

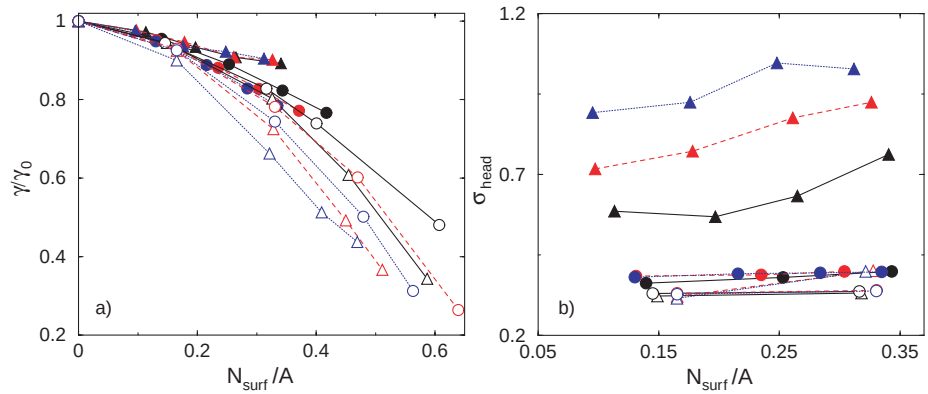

Fig. 3 – a) Reduced interfacial tension (γ/γ_0) as a function of the surfactant concentration at the interface ($N_{\rm surf}/A$) for some single-tail ($\rm ht_4$, $\rm ht_6$, $\rm ht_8$) and double-tail ($\rm h(t_2)_2$, $\rm h(t_3)_2$, $\rm h(t_4)_2$) surfactants with high and low oil-head repulsion $a_{\rm oh}$. The circles are for the single-tail surfactants and the triangles for the double-tail isomers, the open symbols indicate $a_{\rm oh} = 80$ and the filled symbols $a_{\rm oh} = 30$. The surfactants have 4 (black, solid lines), 6 (red, dashed lines), and 8 (blue, dotted lines) tail beads. b) Ordering at the interface as a function of the concentration of molecules at the interface. The ordering is quantified as the width of the distribution, $\sigma_{\rm head}$, of surfactant head groups at the interface.

low concentration we see that the different surfactant structures cause a similar reduction of the interfacial tension. At these low interfacial concentrations the surfactants do not interact and form a two-dimensional ideal gas at the interface. At higher concentrations the surfactants interact and we observe differences between the various structures. For single-tail surfactants (open circles), increasing the tail length results in more efficient surfactants, because of the increased excluded-volume interactions between the tails [19]. Our simulations show that double-tail surfactants, depending on the oil-head interactions, can be either more or less efficient compared to their single-tail isomers. For high values of the oil-head repulsion parameter $a_{\rm oh} = 80$ we find the double-tail isomers to be more efficient, while for $a_{\rm oh} = 30$ we find the single-tail isomers to be more efficient.

To obtain a molecular understanding of the results we investigate the ordering and packing of the surfactants at the interface. A schematic picture of these results is shown in fig. 4. We have computed the width of the distribution of the head groups normal to the interface. Figure 3b) shows that for both the single-tail and double-tail surfactants decreasing the oil-head repulsion results in a broader distribution but this effect is much more pronounced for double-tail molecules. We also investigated the degree of alignment of the bond between hydrophilic and hydrophobic beads with the interfacial normal. The double-tail surfactants lose more bond order than the single-tail isomers when the repulsion parameter is lowered (not

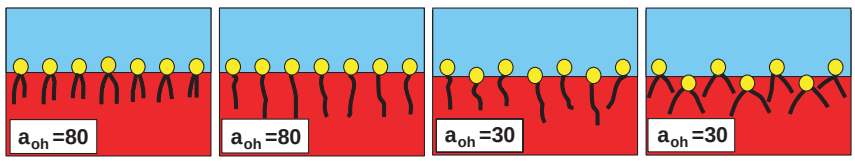

Fig. 4 – Schematic picture of singe-tail and double-tail surfactants at the oil/water interface. The four surfactant types are arranged from left to right in order of decreasing efficiency.

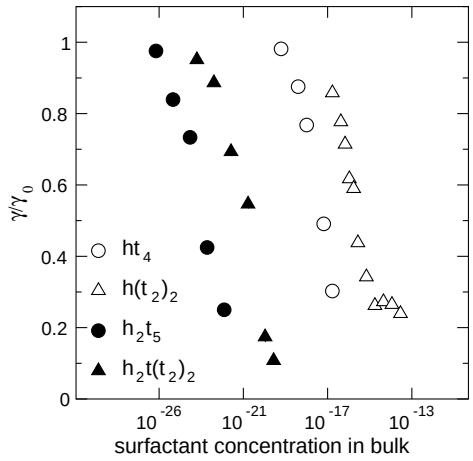

Fig. 5 – Reduced interfacial tension (γ/γ_0) as a function of the bulk surfactant concentration ($N_{\rm surf}/V$) in the water phase for $a_{\rm oh} = 80$.

shown). Inspection of the snapshots of the simulation shows that the molecular explanation of the broadening and the loss of bond order is that the molecules with less hydrophobic headgroups stagger at the interface, as shown schematically in fig. 4. In such an arrangement the excluded-volume interactions are far less efficient in reducing the interfacial tension.

If the oil-head interaction is sufficiently repulsive, the surfactants order nicely at the interface. The distribution of the head groups normal to the interface is narrow and the double-tail molecules experience stronger excluded-volume interactions than the single-tail ones. If the oil-head interaction is decreased, the double-tail molecules stagger, resulting in weaker excluded-volume interactions between them compared to the single-tail isomers. Hence, if we use surfactants with sufficiently hydrophilic head groups, double-tail surfactants are more efficient than single-tail ones for a given interfacial concentration. It is interesting to compare our results with the theoretical calculations [3, 19]. In these theories the head groups are assumed to be in a fixed plane (*i.e.* fig. 4, left). With this assumption, the surfactants are not allowed to adopt a staggered conformation (*i.e.* fig. 4, right).

Interfacial tension vs. bulk concentration. – When we compare the interfacial tension as a function of the bulk concentration of surfactants the picture changes. Figure 5 shows that although the double-tail isomers are more efficient for a given *interfacial* concentration, they are less efficient for a given *bulk* concentration.

The reason for this is as follows: At a given interfacial concentration the effective repulsion between the tails is higher compared to their single-tail isomers (see fig. 4). As a consequence, the chemical potential of these double-tail isomers is significantly higher for the same interfacial concentration. However, in bulk water the Henry coefficient is of the same order of magnitude for single-tail and double-tail molecules. This implies that the concentration of double-tail surfactants in the bulk water phase must be much higher to yield the same (equilibrium) concentration at the interface. At this point, it is important to note that our results on the efficiency should not be confused with the *effectiveness* of a surfactant, defined as the lowest interfacial tension that can be reached by adding surfactant. The effectiveness is usually determined by the interfacial tension at the critical micelle concentration (CMC). If the CMC for a double-tail surfactant is much higher compared to its single-tail isomer, lower interfacial tension can be obtained by using double-tail surfactants.

For the models we have studied, the efficiency at the interface of the double-tail surfactants did not compensate for the reduced ease of adsorption. It is therefore tempting to conclude that it is not possible to synthesize double-tail surfactants that require a lower bulk concentration to reduce the interfacial tension by the same amount as their single-tail isomers. Of course, in our model we have coarse-grained all interactions into very simple potentials. In this process we may have lost the subtleties that may make real double-tail surfactants more efficient than their single-tail isomers.

Summary. – We have shown that a bulk solution in equilibrium with an interface can be simulated using a constant $\mu_{\text{surf}}PT$ ensemble. Moreover, the ordering of head groups normally to the interface can explain why branching of the hydrophobic tail can have either a positive or a negative effect on a surfactant's tension-reducing abilities. Finally, for double-tail surfactants there are two opposing effects: the more efficient the surfactants are at the interface, the higher the bulk concentrations required to get them to the interface.

* * *

These investigations are supported in part by the Norwegian Research Council (grant no. 145184/432), by the Netherlands Research Council for Chemical Sciences (CW), and by the Netherlands Organization for Scientific Research (NWO) through PIONER.

REFERENCES

[1] Tsujii K., *Surface Activity: Principles, Phenomena, and Applications* (Academic Press, San Diego) 1998.
[2] Traube J., *Samml. Chem. Vortr.*, **4** (1899) 255.
[3] van Os N. M., Rupert L. A. M., Smit B., Hilbers P. A. J., Esselink K., Böhmer M. R. and Koopal L. K., *Colloids Surf. A*, **81** (1993) 217.
[4] Klopfer K. J. and Vanderlick T. K., *Colloids Surf. A*, **96** (1995) 171.
[5] Varadaraj R., Bock J., Valint P. jr., Zushma S. and Thomas R., *J. Phys. Chem.*, **95** (1991) 1671.
[6] Pitt A. R., Morley S. D., Burbidge N. J. and Quickenden E. L., *Colloids Surf. A*, **114** (1996) 321.
[7] Wormuth K. R. and Zushma S., *Langmuir*, **7** (1991) 2048.
[8] Aspée A. and Lissi E, *J. Colloid Interface Sci.*, **178** (1996) 298.
[9] Ghaïcha L., Leblanc R. M. and Chattopadhyay A. K., *J. Phys. Chem.*, **96** (1992) 10948.
[10] Green S. R., Su T. J., Lu J. R. and Penfold J., *J. Phys. Chem. B*, **104** (2000) 1507.
[11] Hoogerbrugge P. J. and Koelman J. M. V. A., *Europhys. Lett.*, **19** (1992) 155.
[12] Frenkel D. and Smit B., *Understanding Molecular Simulations: from Algorithms to Applications*, 2nd edition (Academic Press, San Diego) 2002.
[13] Prinsen P., Warren P. B. and Michels M. A. J., *Phys. Rev. Lett.*, **89** (2002) 148302.
[14] Groot R. D., *Langmuir*, **16** (2000) 7493. To obtain similar bulk densities for the water and oil phase we used $a_{\text{oo}} = 25$ instead of 15 used by Groot.
[15] Groot R. D. and Rabone K. L., *Biophys. J.*, **81** (2001) 725.
[16] Smit B., *Phys. Rev. A*, **37** (1988) 3431.
[17] Smit B., Schlijper A. G., Rupert L. A. M. and van Os N. M., *J. Phys. Chem.*, **94** (1990) 6933.
[18] Frenkel D., Mooij G. C. A. M. and Smit B., *J. Phys. Condens. Matter*, **4** (1992) 3053.
[19] Szleifer I., Ben-Shaul A. and Gelbart W. M., *J. Phys. Chem.*, **94** (1990) 5081.

Paper II

Investigation of Surfactant Efficiency Using Dissipative Particle Dynamics

Live Rekvig[1], Marieke Kranenburg[2], Jocelyne Vreede[2], Bjørn Hafskjold[1], Berend Smit[2]

[1]Department of Chemistry, Norwegian University of Science and Technology N-7491 Trondheim, Norway
[2]Department of Chemical Engineering, University of Amsterdam Nieuwe Achtergracht 166, 1018 WV Amsterdam, The Netherlands

Abstract

We have used dissipative particle dynamics (DPD) to simulate surfactant monolayers on the interface between oil and water. With a simple surfactant model, we investigate how variations in size and structure of surfactants influence their ability to reduce the interfacial tension. In particular, we studied the effect of branching of the hydrophobic tail. We found that branched surfactants are more efficient at the interface than linear ones only if the head groups are sufficiently hydrophilic to prevent the molecules from staggering. By combining DPD with a Monte Carlo method, we have imposed constant surfactant chemical potential and (normal) pressure in separate simulations of bulk and interface. From this, we can determine the bulk concentration needed to obtain a given interfacial tension. We found that higher concentrations of branched surfactants are required to obtain the same reduction of the interfacial tension. We argue that the stronger excluded volume interactions which make branched surfactants more efficient at the interface compared to their linear isomers at the same time make them less inclined to adsorb at the interface.

Published in *Langmuir*, vol. 19, pages 8195–8205, year 2003.

Paper III

JOURNAL OF CHEMICAL PHYSICS VOLUME 120, NUMBER 10 8 MARCH 2004

Simulating the effect of surfactant structure on bending moduli of monolayers

Live Rekvig[a] and Bjørn Hafskjold
Department of Chemistry, Norwegian University of Science and Technology, N-7491 Trondheim, Norway

Berend Smit
Department of Chemical Engineering, University of Amsterdam, Nieuwe Achtergracht 166, 1018 WV Amsterdam, The Netherlands

(Received 30 October 2003; accepted 10 December 2003)

We have used dissipative particle dynamics to simulate amphiphilic monolayers on the interface between oil and water. An ultralow interfacial tension is imposed by means of Monte Carlo to resemble the amphiphilic films that separate oil and water regions in microemulsions. We calculate the bending modulus by analyzing the undulation spectrum. By varying the surfactant chain length and topology we investigate the effect of surfactant structure and composition of the monolayer on the bending moduli. We find that increasing the thickness has a larger effect than increasing the density of the layer. This follows from the observations that at a given interfacial tension, the bending modulus increases with chain length and is larger for linear than branched surfactants. The increase with chain length is approximately linear, which is slower than the theoretical predictions at a fixed area. We also investigated a binary mixture of short and long surfactants compared to pure layers of the same average chain length. We find a roughly linear decrease in bending modulus with mole fraction of short surfactants. Furthermore, the mixed film has a lower bending modulus than the corresponding pure film for all mole fractions. Linking the bending moduli to the structure of the surfactants is an important step in predicting the stability of microemulsions. © *2004 American Institute of Physics.* [DOI: 10.1063/1.1645509]

I. INTRODUCTION

The interaction between two interfaces of amphiphilic molecules is of importance in many systems: Membrane–membrane interaction in biological systems is one example,[1] another is microemulsions.[2,3] Microemulsions are surfactant-rich emulsions where hydrophilic and hydrophobic regions are so well mixed that the interfaces dominate. They can take on many structures such as water droplets in oil, oil droplets in water, spongelike, bicontinuous structures, and lamellar phases. To better understand the behavior of such systems we would like to relate the mesoscopic properties of the interface to the structure of the surface active molecules which constitute the interface. The relation goes via a description of the interfacial properties: the interfacial tension and the elastic constants. These properties describe the energy of an interface with a given area and principal curvatures c_1 and c_2,[4]

$$E=\int dA\left(\gamma+\frac{\kappa}{2}(c_1+c_2-2c_0)^2+\bar{\kappa}c_1c_2\right). \tag{1}$$

Here, γ is the interfacial tension, κ is the bending modulus, $\bar{\kappa}$ is the saddle-splay (Gaussian) modulus, and c_0 is the spontaneous curvature. Previously we investigated the dependence of the interfacial tension γ on surfactant structure.[5] Here we examine how this structure influences the bending modulus κ.

The energy of an interface is, to a first approximation, characterized by its interfacial tension, which is a measure of the energy cost of increasing the interfacial area by one unit. For interfaces between oil and water, or air and water, the tension will normally be high and the two phases will be well separated. Furthermore, the interfaces are essentially flat on the scale involving hundreds of molecules. The interfacial tension can however be substantially lowered by adding a surfactant. The surfactant molecules will adsorb on the interface with their hydrophilic part in the water phase and the hydrophobic part in the oil phase. When the surfactant coverage is high, the energy cost of increasing the area of an interface can become very low. Under these circumstances the bending modulus becomes important. κ characterizes the resistance of the interface towards bending. A low bending modulus means large thermal undulations. Such fluctuations give rise to entropic repulsive forces between two interfaces close to each other such as two bilayers in lamellar phases or two monolayers separating the oil and water regions in a microemulsion.[6] Microemulsions are characterized by low interfacial tension. Their phase (oil-in-water, water-in-oil, lamellar, or bicontinuous) is therefore largely dictated by the spontaneous curvature and bending modulus.[7]

Experimentally, κ can be determined using high-resolution scattering techniques.[8] The spectrum of undulation modes is measured and fitted to the spectrum predicted by the Hamiltonian model Eq. (1). It is now possible to compute κ in molecular dynamics simulations in much the same way. This was first done by Goetz *et al.*[9] who studied a lipid bi-

[a]Author to whom correspondence should be addressed. Electronic mail: live.rekvig@phys.chem.ntnu.no

layer. They found two regimes: The spectral intensity of wave lengths on the molecular scale (protrusion modes) scaled as q^2, where $q=2\pi/\lambda$ and λ is the undulation wavelength. The intensity of the longest wave lengths scaled as q^4, and from the intensity of these modes, κ was extracted.

Whereas Goetz *et al.* used an iterative procedure to find the area corresponding to a tensionless membrane, Lindahl and Edholm[10] employed a pressure scaling scheme to simulate a tensionless bilayer. This study showed an anticorrelation between area fluctuations and the intensity of undulatory modes. It therefore seems natural to use a simulation scheme that includes the natural area fluctuations when sampling the undulation spectrum. Several computational studies of bilayer rigidity have followed.[11–13] Laradji and Mouritsen[14] studied a monolayer on the oil/water interface with molecular dynamics. Using symmetric surfactants and special boundary conditions, they investigated the effect of surfactant density on γ and κ. They found that κ decreases with increasing surfactant density for low densities but increases with further increase of the surfactant density.

A few theoretical studies based on the mean-field approach have addressed the effect of structure and composition on the elastic constants in detail.[15–19] The results differ qualitatively with respect to the dependence of κ on chain length and on mole fractions of cosurfactants. The theoretical approaches differ in a few respects; one of the differences being fixed area versus fixed interfacial tension. In this paper we describe large scale particle simulations that further investigate these issues.

Previous simulation studies used molecular dynamics[9,10,14] with a united atoms model[10] or a Lennard-Jones based model.[9,14] In this simulation study we use a more coarse-grained approach: A simple model of head, tail, water, and oil beads captures the essential properties of ternary systems such as phase separation and adsorption. Changes in surfactant structure such as chain length and branching can easily be realized. We calculate bending moduli for a variety of surfactant structures and binary mixtures of surfactants. The aim is a molecular understanding of the bending modulus. This is important because it is agreed that the bending modulus is a key parameter in understanding structure and phase behavior of microemulsions.[20]

We have chosen a coarse-grained method, dissipative particle dynamics (DPD) to govern the particle dynamics. The advantage of DPD over molecular dynamics is that the accessible time and length scales are increased by approximately an order of magnitude. We use a Monte Carlo technique to vary the box shape during the simulations according to a specified constant interfacial tension.[21] In this manner we can compare the bending moduli for monolayers at the same interfacial tension, resembling saturated, low-tension layers such as in a microemulsion.

II. MODEL AND SIMULATION DETAILS

A. Dissipative particle dynamics

In DPD, conservative, random, and dissipative forces act between two particles i and j which are a distance r_{ij} apart,

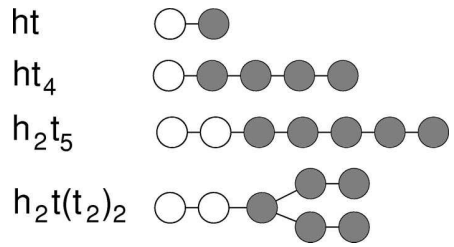

FIG. 1. Some of the model surfactants investigated in this study and the nomenclature used. The white particles are hydrophilic beads (h) and the gray particles hydrophobic tails (t).

$$\mathbf{F}_{ij}=\mathbf{F}_{ij}^{C}(r_{ij})+\mathbf{F}_{ij}^{R}(r_{ij})+\mathbf{F}_{ij}^{D}(r_{ij}), \tag{2}$$

where the forces are of the form

$$\mathbf{F}_{ij}^{C}=a_{ij}w^{C}(r_{ij})\hat{\mathbf{r}}_{ij}, \tag{3}$$

$$\mathbf{F}_{ij}^{R}=\sigma w^{R}(r_{ij})\theta_{ij}\hat{\mathbf{r}}_{ij}, \tag{4}$$

$$\mathbf{F}_{ij}^{D}=-\eta w^{D}(r_{ij})(\hat{\mathbf{r}}_{ij}\cdot\mathbf{v}_{ij})\hat{\mathbf{r}}_{ij}. \tag{5}$$

Here, $\mathbf{v}_{ij}$ is the velocity difference for the two particles, $\hat{\mathbf{r}}_{ij}$ is the unit vector pointing from particle i to particle j. θ is a random number between 0 and 1, a_{ij}, σ and η determine the amplitude of the conservative, random and dissipative forces, respectively, while the w's are weight functions. To obey the fluctuation-dissipation theorem, we must have $w^D=(w^R)^2$, and the system temperature will follow from the relation between σ and η: $\sigma^2/\eta=2kT$.[22] We use the same integration algorithm, weight functions, and parameters as Groot and Warren,[23]

$$w^{C}(r)=w^{R}(r)=\sqrt{w^{D}(r)}=w(r), \tag{6}$$

where

$$w(r)=\begin{cases}1-\dfrac{r}{r_c} & \text{for } r<r_c\\ 0 & \text{for } r\geqslant r_c.\end{cases} \tag{7}$$

Throughout this paper we use reduced units. r_c is the unit of length, kT (the temperature of the thermostat) is the unit of energy, and the mass unit is the mass of a DPD bead. In these units, $\sigma=3.0$ and $\eta=4.5$.

B. Model

We use a coarse-grained approach where one DPD-particle represents a group of atoms, or a liquid volume. Water beads, oil beads, head groups, and tail groups are denoted by w, o, h, and t, respectively. The tail beads are identical to the oil beads. Some of the model surfactants investigated are shown in Fig. 1. A surfactant molecule consists of head groups and tail groups connected by harmonic springs:

$$\mathbf{F}_{ij}^{\text{Bond}}=-k_s(r_{ij}-r_0)\hat{\mathbf{r}}_{ij}. \tag{8}$$

We choose $k_s=100$ and $r_0=0.7$. Water and oil are represented by a single bead for simplicity. One tail bead typically represents a few CH_2 groups.[24–26] The repulsion parameters used are shown in Table I. These are taken from Groot,[25]

TABLE I. Repulsion parameters a_{ij}. w=water bead, o=oil or tail group, and h=head group.

	w	o	h
w	25	80	15
o	80	25	80
h	15	80	35

except that we used $a_{oo}=25$ instead of 15. This change has been made to obtain similar bulk densities in the oil and in the water phase (see also Ref. 5).

C. Simulation details

The systems contained typically 32 000 beads. The number of surfactant molecules used varied from 600 for the largest and up to 1400 for the smallest, of which not all are at the interface. This gave equilibrium areas of typically 22×22. Periodic boundary conditions were applied in all three directions. All simulations were performed at a bead density of 3.0 and with a time step of 0.03.

After an equilibrium area was reached, each system was simulated for at least 8000 Monte Carlo steps. Each Monte Carlo step consists of either a series of DPD steps (between 1 and 200 with equal probability) or an attempt to change the box shape.

Figure 2 shows a snapshot of two monolayers with a total of 618 h_2t_5 surfactant molecules. The 16 000 oil beads and 16 000 water beads are not shown for clarity. Due to the high repulsion between hydrophilic and hydrophobic beads (Table I) all the surfactant molecules are at the interfaces. If the interfacial tension is very low, the film is not strictly flat and undulatory waves can be observed.

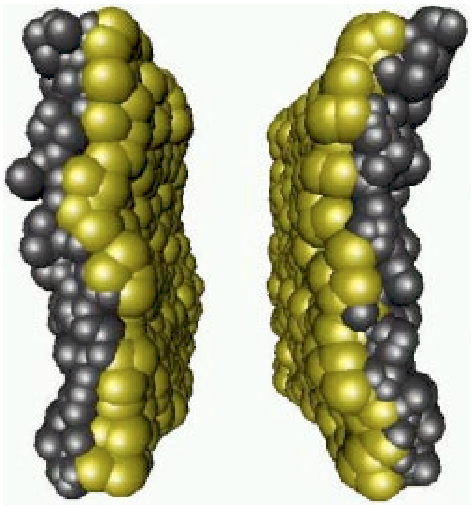

FIG. 2. Snapshot of 618 h_2t_5 surfactant molecules at zero interfacial tension. Head beads are in yellow and tail beads in gray. The head beads have been drawn larger compared to the tail beads to visualize the high head–head repulsion. Water (in the middle) and oil (on the sides) have been omitted for clarity. [Picture prepared with VMD (Ref. 27).] (Color online only.)

D. Constant $N\gamma T$ conditions

We perform most simulations in a constant $N\gamma T$ ensemble. The monolayers in microemulsions usually have ultralow interfacial tensions, but the area per surfactant molecule may vary depending on the surfactant. A constant γ is thus a better reference state than constant area per molecule when comparing with experiments. Also, it is hard to impose a given area per molecule because not all surfactant molecules are necessarily at the interface; some may form micelles or dissolve in water.

By simulating a constant $N\gamma T$ ensemble we allow for the natural local area fluctuations in real systems. Lindahl and Edholm found that area fluctuations and undulations are weakly anticorrelated.[10] This indicates that area fluctuations may influence the undulation intensity. We will therefore compare the constant area and constant interfacial tension schemes in Sec. II G.

Constant interfacial tension is achieved in the simulations by combining DPD with a Monte Carlo scheme.[28] The box volume is kept constant while the shape of the box is allowed to fluctuate according to the specified γ.[21]

For surfactants on an oil/water interface, the interfacial tension depends on the amount and the type of surfactant. We find that $\gamma=0$ can be obtained with surfactants as small as ht_3. Starting the simulation with a large area, the area will decrease until the surfactant density at the interface corresponds to that of zero interfacial tension. The tensionless interface will coexist with surfactant molecules dissolved in bulk or micelles. For ht and ht_2 surfactants $\gamma=0$ could not be obtained. When imposing a too low interfacial tension in the simulations, an equilibrium box area cannot be established. The area continues to decrease while the surfactant molecules migrate into the water phase and eventually form various aggregates.

E. Undulatory fluctuations

To compute the bending moduli we analyze the fluctuations of the interface. The first step is to characterize the interface. For a sufficiently large number of surfactant molecules the interface can be described by continuum theory.[4] Let $h(x,y)$ be the local displacement from the average position of the interface, $h(x,y)=z(x,y)-z_0$, where z is the direction normal to the interface and z_0 is the average position of the interface. We will now rewrite Eq. (1) in terms of $h(x,y)$ as $h(x,y)$ can be monitored easily in the simulations. For small curvatures, $c_1+c_2=\nabla^2 h$ and $dA=dxdy\sqrt{1+(\nabla h)^2}$. For now we assume $c_0=0$ in Eq. (1). The surface integral over c_1c_2 is constant when the topology does not change, specifically, it is zero for a film.[29] This implies that $\overline{\kappa}$ does not affect the energy fluctuations in a monolayer and henceforth not the calculations of the bending moduli. It also means that this elastic constant can not be determined by studying a given topology as in this study. The leading terms in curvature become[30]

$$e(h(x,y))\equiv(E(h(x,y))-E(0))/A \tag{9}$$

$$=\frac{\gamma}{2}(\nabla h(x,y))^2+\frac{\kappa}{2}(\nabla^2 h(x,y))^2. \tag{10}$$

While the last term is the energy cost related directly to the bending of the monolayer, the first term on the right describes the energy cost due to an increase in area upon bending. Fourier transformation of Eq. (10) gives

$$\tilde{e}(\tilde{h}(q)) = \frac{\gamma}{2} q^2 \tilde{h}(q)^2 + \frac{\kappa}{2} q^4 \tilde{h}(q)^2. \tag{11}$$

According to the equipartition principle,

$$\langle \tilde{e}(\tilde{h}(q)) \rangle = \frac{1}{A} \frac{k_B T}{2} \tag{12}$$

such that

$$\langle |\tilde{h}(q)|^2 \rangle = \frac{k_B T}{A} (\gamma q^2 + \kappa q^4)^{-1}. \tag{13}$$

For short wavelengths the continuum picture is not valid. Molecular protrusions characterize the interface and these will be described by a protrusion tension σ similar in nature to the interfacial tension,[10]

$$\langle |\tilde{h}(q)|^2 \rangle = \frac{k_B T}{A} (\sigma q^2)^{-1}. \tag{14}$$

Because we have applied a coarse-grained surfactant model, we will not investigate the interface at this level of detail.

Equation (13) predicts the spectral intensities of each undulation mode as a function of wave vector q. From the simulation we can obtain $\langle |\tilde{h}(q)|^2 \rangle$ by monitoring $h(x,y)$ and by fitting the results to Eq. (13), the elastic constants can be estimated.

F. Spectral analysis

To perform spectral analysis we need to monitor the local position $z(x,y)$ of each of the two interfaces. Note that we treat the two monolayers separately. The periodic boundary conditions prohibit simulation of a single monolayer between oil and water. A grid with 30×30 points was assigned to each interface. In the systems with high concentration of surfactants we defined the position of the interface locally from the positions of the surfactant head groups connected to the first tail bead. Two practical problems arise: First, how to determine whether a surfactant molecule belongs to one of the two interfaces or not. If it is dissolved in the bulk phases or is part of a micelle it should be disregarded when the position of the interface is calculated. Second, for each grid point (i,j), the position $z(i,j)$ must be defined as some (weighted) average of the z-coordinates of the surfactant head groups nearby.

To determine which surfactant molecules belong to the interface, we used a cluster algorithm with the following criteria: Given two cut-off parameters R_{xy} and R_z, two molecules a and b belong to the same cluster if

(1) $(z_a^h - z_b^h)^2 < R_z^2$,
(2) $(x_a^h - x_b^h)^2 + (y_a^h - y_b^h)^2 < R_{xy}^2$,
(3) $(z_a^t - z_b^t)^2 < R_z^2$,
(4) $(x_a^t - x_b^t)^2 + (y_a^t - y_b^t)^2 < R_{xy}^2$,
(5) $(z_a^h - z_a^t)/|z_a^h - z_a^t| = (z_b^h - z_b^t)/|z_b^h - z_b^t|$,

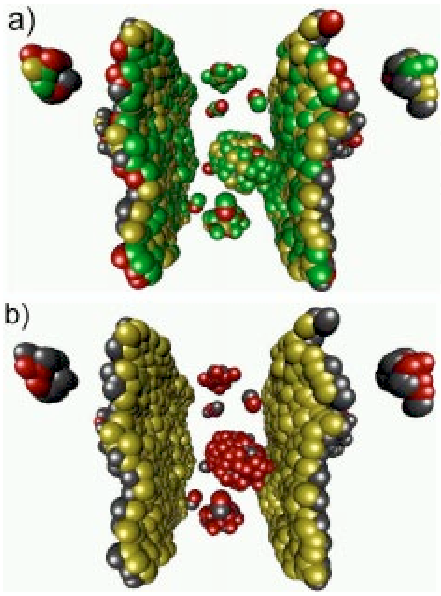

FIG. 3. Snapshots from a system with 50% ht_5 and 50% ht surfactant at interfacial tension $\gamma = 0.1\gamma_0$. Only the head groups and the first tail bead (the one connected to the head) are shown. The head beads have been drawn larger compared to the tail beads to visualize the high head–head repulsion. Water (in the middle) and oil (on the sides) as well as the four last tail beads of ht_5 have been omitted for clarity. (a) and (b) represent the same configuration. In (a) beads are colored according to type: ht_5 heads in yellow, ht_5 tails in gray, ht heads in green, and ht tails in red. In (b) the head groups are colored yellow if they are assigned to the interface and red otherwise. [Picture prepared with VMD (Ref. 27).] (Color online only.)

where superscript h denotes the head bead closest to the tail and t the tail bead closest to the head. The four first criteria ensure that both the two head groups and the two tail groups are close. The last criterion states that their head–tail bonds must have the same direction projected onto the interfacial normal. This is efficient in filtering out single surfactant molecules or micelles very close to the interface. Different values for the parameters R_z and R_{xy} were used depending on the type of surfactant(s). This involved some trial and error until the two largest clusters correctly included all and only those surfactant molecules making up the interface. Visual inspection of snapshots in which molecules belonging to the two largest clusters were color-marked served as a final check. Typical values that gave a good description of the interface were $R_z = 0.9 - 1.1$ and $R_{xy} = 1.8 - 2.1$. For each surfactant type and density, we found a range in which small variations δ of R_z and R_{xy} did not affect the number of surfactant molecules in the interface. Then all the surfactant molecules at the interfaces are included in the cluster and those that are a distance between R_z and $R_z + \delta$ away are filtered out with the bond direction criterion anyway.

Figure 3 shows an example configuration with 50% ht_5 and 50% ht surfactant at $\gamma = 0.1\gamma_0$ where $\gamma_0 = 3.45$ is the bare oil–water interfacial tension. Only the head groups and the tail groups attatched to them are shown for clarity. The small surfactant molecules are soluble in water and there are also a few micelles. In Fig. 3(a) the head groups of the large and small surfactant molecules are shown in yellow and green, respectively, the tails are in gray and red. In Fig. 3(b)

the surfactants are colored according to the outcome of the cluster analysis: Surfactants that are determined to be part of the interface have yellow head groups, while the rest have red head groups.

The position $z(i,j)$ must be defined as some function of the z-coordinates of surfactant molecules close to the grid point, for example,

$$z(i,j)=\frac{\Sigma_k r_k^{-p} z_k}{\Sigma_k r_k^{-p}}, \tag{15}$$

where $r_k=(x_k-\Delta i)^2+(y_k-\Delta j)^2$ and the sum is over all surfactant molecules that have $r_k<R$. R must be large enough such that at least one molecule is assigned to the grid point but small enough such that $z(i,j)$ is indeed the *local* position. A high p gives the molecules close to the grid point more weight. We chose $p=5$ and R around unity to get 1–4 surfactant molecules within R. We find that the values chosen for R, p and the number of grid points affect the intensity of the highest q-modes (protrusion modes). However, they have only a negligible effect on the low q-modes from which we determine the bending modulus.

For the systems with few or zero surfactant molecules (the first four points in Fig. 5 below) the interface could not be described by the surfactants alone so we used a different definition of the interface. We let all pairs consisting of one hydrophobic and one hydrophilic bead which were closer than r_c contribute to the interface. Now all surfactant molecules are at the interfaces so no cluster routine was needed. The assignment of positions to grid points were done in the same way as for high surfactant concentrations.

The two-dimensional discrete Fourier transformation yields

$$\tilde{h}(i_q,j_q)=\sum_{i=0}^{n-1}\sum_{j=0}^{n-1} h(i_r,j_r)\exp\left\{\frac{-2\pi i}{n}(i_r i_q+j_r j_q)\right\}. \tag{16}$$

We can replace $h(i_r,j_r)$ by $z(i_r,j_r)$ in Eq. (16) as the constant z_0 vanishes in the summation. After averaging $\tilde{h}(i_q,j_q)$ over all snapshots we can obtain $\tilde{h}(q_r)$ for $q_r=\sqrt{(i_q^2+j_q^2)}2\pi/L_x$, where L_x is the average box size in x and y direction and $(i_q^2+j_q^2)\leqslant(n-1)^2$.

Figure 4 shows the spectral intensity $S(q)=\langle|\tilde{h}(q)|^2A\rangle$ versus $q=2\pi/\lambda$, where A is the average box area and λ is the undulation wave length for h_2t_5 surfactants at $\gamma=0$. The full line in Figs. 4(a) and 4(c) represents $S(q)=1/(3.3q^4)$. The agreement with Eq. (13) is very good: At long wavelengths, the continuum picture is valid and $S(q)=1/(\kappa q^4)$. In the log/log plot we can identify q^{-4} behavior for low q values and a transition towards q^{-2} behavior for high q. When plotting $1/(S(q)q^2)$ versus q^2 we get a straight line in the continuum regime, where κ is the slope and γ is the crossing with the y-axis.

The box dimensions limit the lowest q mode we can measure to $q_{\min}=2\pi/\sqrt{A}$. We stress that Eq. (13) is valid in the continuum limit so $1/(S(q)q^2)$ versus q^2 is only linear in the limit $q\to 0$. This means that there is some uncertainty in the extrapolation needed to determine κ. Thus a systematic error due to the finite system size might add to the statistical

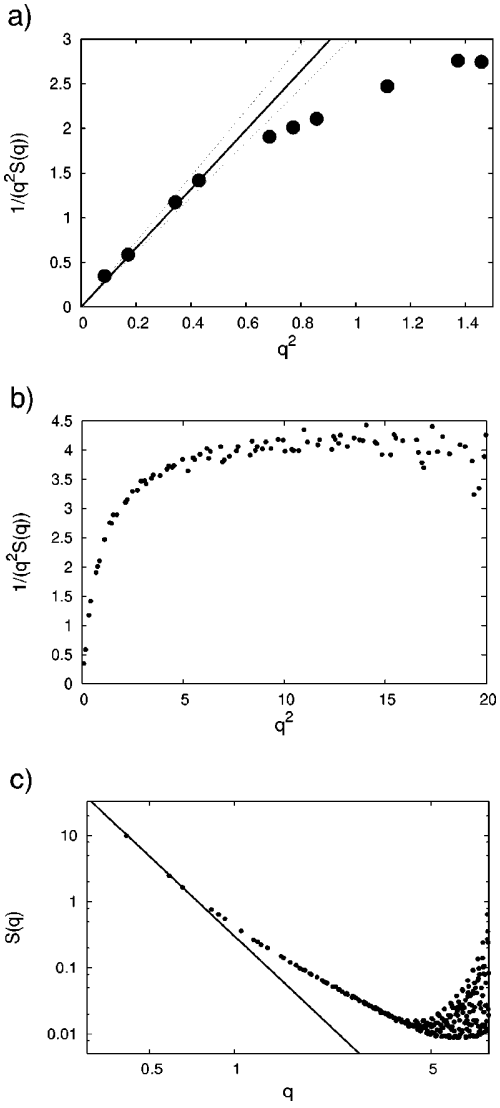

FIG. 4. Spectral intensities for h_2t_5 at $\gamma=0$. The slopes of the full and dotted lines represent the values for κ and the lower and upper error bars in Fig. 11, respectively.

errors shown in the plots. All κ values reported here have been calculated by fitting the first four points (weighted by their statistical errors) to $y=\gamma+\kappa x$. The reported error bars include results and uncertainties if we fit to three or five points.

G. Comparison between constant γ and constant *A* simulations

To compare the results and accuracy in the constant interfacial tension and the constant area ensemble, we studied the dependence of κ on interfacial density for the ht_4 surfactant. First we performed constant area simulations with various surfactant concentrations. We sampled the interfacial tension and continued the simulations imposing this interfacial tension. We found no difference in results between the two ensembles within the uncertainty of the results (see Fig. 5 in Sec. III A). However, the accuracy differs. Because the constant interfacial tension is more time consuming, the *NVT* ensemble is more efficient for a given CPU time, but

for a given number of DPD steps, the $N\gamma T$ ensemble gives better accuracy. This is mainly because there is no uncertainty in γ, and the accuracy of γ influences the accuracy in κ when fitted to Eq. (13).

We perform most simulations in the $N\gamma T$ ensemble to compare different structures and compositions at the same (zero or very low) interfacial tension, resembling saturated monolayers and microemulsion conditions.

H. Asymmetric surfactants

Equation (10) is valid for interfaces where the preferred curvature is zero, for example bilayers or monolayers of surfactants which are symmetric in the sense that they do not prefer to bend towards either the oil or the water phase. The surfactants studied here are, like most real surfactants, asymmetric. However, in a simulation with periodic boundary conditions the interfaces are constrained to be flat on average. This means that the average curvature, $\overline{c}=\langle c_1+c_2\rangle/2=0$, differs from the preferred curvature c_0 which is determined by the characteristic volume v_0, chain length l_s and head group area a_0 of the surfactant.[4]

The replacement of c_0 with $\overline{c}$ in Eq. (1) may in general lead to a distribution of modes differing from Eq. (13). This would be observed in the fluctuation spectrum with $S(q)$ differing from Eq. (13). Since the model fits the spectrum well, we neglect this error. Specifically, we can check the q^2 dependence since the interfacial tension is imposed and can also be calculated independently from the pressure tensor.[31] We obtain the interfacial tension on the y-axis within the errors by extrapolating the linear part to $q=0$ [Fig. 4(a)]. We conclude that Eq. (13) is a good description of the fluctuation spectrum within the uncertainties of the method.

In real microemulsions where $\overline{c}\neq 0$ curvature fluctuations appear as deviations in droplet shape and size from spheres with radius c_0^{-1}. The size and shape fluctuations can be described in terms of spherical harmonics.[32,33] That allows experimentalists to extract the bending moduli from analyzing the neutron scattering on microemulsion droplets.[20,34] Those bending moduli describe the energy cost of curvature deviations away from the average droplet size with radius c_0^{-1}. The bending moduli reported here describe instead the average energy cost of curvature deviations away from a *flat* surface.

III. RESULTS AND DISCUSSION

We will here determine how the bending modulus depends on the molecular structure and composition of surfactants. First we investigate the dependence on density for a simple linear surfactant (Sec. III A). This is done using both the constant area and constant interfacial tension ensembles for comparison. The remaining simulations will be at a constant low interfacial tension to resemble the conditions in microemulsions. We use $\gamma=0$ or $\gamma=0.1\gamma_0$ where $\gamma_0=3.45$ is the bare oil–water interfacial tension.

A. Effect of surfactant density

For the linear surfactant ht_4 we studied the dependency on interfacial density. We performed both constant area simulations and constant interfacial tension simulations. Figure 5 shows that the bending modulus increases monotonously with increasing density of surfactant. While the area fluctuations increase with increasing density due to lower interfacial tension, *bending* the sheet becomes increasingly energy costly. Without surfactant, bending of the layer has little effect on the packing, only on the area. The bending modulus is therefore very low. With surfactant at the interface, bending involves squeezing of the chains on one side of the layer. Oil and water molecules close to the surface can easily diffuse away from the compressed volume but the surfactant molecules cannot. As their density increases, steric forces due to bending increase accordingly.

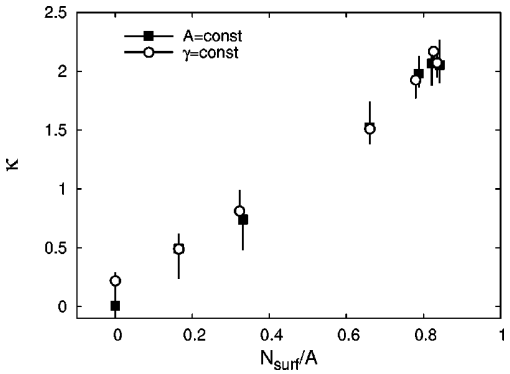

FIG. 5. Bending modulus as a function of surfactant density of ht_4 surfactant. The simulations at constant interfacial tension (circles) are continuations of simulations at constant area (squares), imposing the average interfacial tension from the constant area simulations. Sampling was done during 5×10^5 DPD steps in both cases.

A nonmonotonic dependence of κ with area per surfactant molecule for weak linear surfactants was reported previously.[14] Local fluctuations in the alignment at the interface can decrease the bending modulus from the bare oil/water value. This effect disappears as the density increases and/or as the surfactant molecules become longer or stronger, i.e., when their tendency to align increases. For dense monolayers and/or strong surfactants the tendency to align perpendicular to the interface will increase monotonously with surfactant density. The surfactants investigated in this study, in particular the ht_4 surfactant in Fig. 5, must be regarded as strong surfactants in the sense that the solubility in water[5] is very low. Because of the coarse-graining they represent larger surfactants than the Lennard-Jones based four- and eight-beaded surfactants in Ref. 14. This might account for the qualitative difference observed.

B. Effect of chain lengths

We simulated monolayers of linear surfactants of type ht_n, $n=1-6$ in the constant interfacial tension ensemble. A tensionless state could be obtained for $n\geqslant 3$. Figure 6 shows that the bending modulus increases linearly with the number of tail beads. As the monolayer becomes thicker, the energy cost of bending the monolayer increases. For monolayers of surfacants with a given area per molecule, one intuitively expects the energy cost of bending the membrane to increase as the tails become longer. Here we find that this is also true

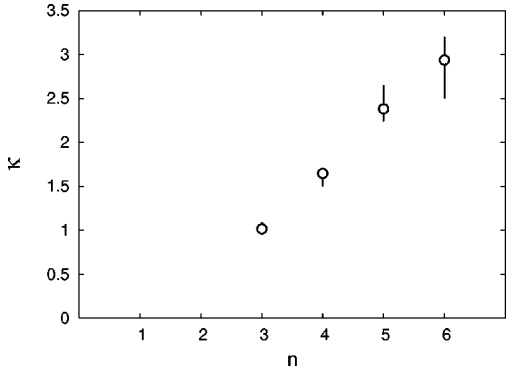

FIG. 6. Bending modulus as a function of the number of tail beads n for ht_n surfactants at $\gamma=0$.

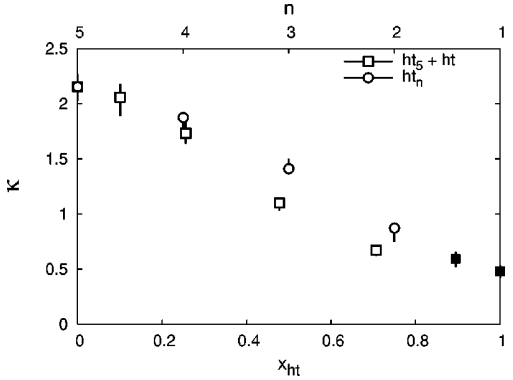

FIG. 7. Bending modulus as a function of mole fraction of cosurfactant added to the ht_5 surfactants (squares, lower x-axis) and as a function of chain length n for pure ht_n surfactants (circles, upper x-axis). The imposed interfacial tension was $\gamma=0.1\gamma_0$ (open symbols) except for $x_{ht}=0.9$ and $x_{ht}=1.0$ which are at $\gamma=0.2\gamma_0$ (solid symbols).

if one compares the different chain lengths at the same interfacial tension rather than interfacial density. This means that the chain length affects bending moduli more than the packing density does. Both $\gamma_0-\gamma$ and κ increase with interfacial density and/or chain lengths. It is, however, interesting to note that κ is more sensitive to these parameters than γ is. For a given increase in chain length, the density can be lowered to give the same γ. κ, however, depends more strongly on chain length than density and will increase unless the density is further decreased.

Figure 6 suggests a linear increase with chain length in the given range. Theory predicts a power-law $\kappa\propto n^p$, $p=2-3$,[4,16] often used as a theoretical reference in experiments.[34–37] However, in the theory the area per molecule is kept constant. That is not the case in our simulations nor in the experimental situation. The rate of increase in Fig. 6 would be higher if one compared different surfactants at a given density rather than at a given interfacial tension. This follows from two observations: The surfactant density at a given interfacial tension increases with increasing tail length,[5] and the bending modulus increases with density for a given chain length (Fig. 5). Our results are in accordance with theory at similar conditions.[17,38]

It is interesting to make a more detailed comparison with the experimental data. A tail bead in our model represents approximately three CH_2 groups. The surfactants in Fig. 6 therefore correspond to chains with 9–18 alkyl units, which are typical lengths of real surfactants. $2\kappa+\bar{\kappa}$ has been measured experimentally for surfactants with number of alkyl units between 8–12 (polyethyleneglycol alkyl ethers[34,36]) and 12–18 (*n*-alkyl-*n*-dodecyldimethylammonium bromides[37] and alkyl amine oxides[36]). The data are fit to power laws with $p=2.3$ and $p=2.95$ grounded on the theoretical prediction at constant area. However, with only 3–4 points for each surfactant type and some scattering in the results they could equally well fit a linear curve in the same range, especially because an investigation towards $n=0$ is impossible both in experiments and simulations (at $\gamma\simeq 0$).

C. Effect of adding cosurfactant

Figure 7 shows the bending modulus as a function of mole fraction of cosurfactant (ht) added to the ht_5 surfactant. Also shown is the effect of reducing the chain length for all the surfactant molecules to the same average. We see that the effect of replacing some long surfactant molecules with short ones is larger than the effect of reducing the chain length of all molecules. A low tension monolayer cannot be obtained with all surfactant types, see discussion in Sec. II D. We therefore used $\gamma=0.1\gamma_0$ except for $x_{ht}=0.9$ and $x_{ht}=1.0$ where we used $\gamma=0.2\gamma_0$. Those two points are therefore slightly higher than the trend in Fig. 7 suggests.

The effect of binary mixture versus single-component monolayer was also investigated using mean-field theory assuming constant area[15,16,19] and assuming saturated monolayers.[17,18] Szleifer *et al.*[15] predicted that the bending modulus of an equimolar mixture could become as low as that of a membrane composed of only the short molecules. Cantor[17] found no pronounced difference between a mixed and pure monolayer at any average chain length. Our results are somewhat in between: A lower κ for the binary mixture, decreasing with mole fraction of the ht surfactant. The calculations in Ref. 17 are carried out under the condition of ''saturated'' monolayers, which is similar to imposing a low interfacial tension. In Ref. 16 the monolayers are compared at a given area, i.e., not accounting for the variation in surface density. It is therefore interesting to note that our simulation results differ qualitatively from both these works.

The suppression of a possible spontaneous curvature c_0 might have an effect on the measured κ. Calculations have shown that the cosurfactant has a larger effect on the curvature than on the bending modulus.[18] Here, a mean curvature of zero is forced through the periodic boundary conditions.

A reduction in bending rigidity with addition of short chain surfactant was also observed experimentally. Gradzielski *et al.* studied a binary mixture of $C_{12}E_5$ and C_8E_2 surfactant (polyethyleneglycol alkyl ethers) and found a trend and values very similar to those in Fig. 7.[36] It was also found that the decrease in κ upon adding cosurfactant depends on the difference in chain length between the short and long surfactants; short surfactants reducing κ more for a given mole fraction.[35,39]

An interesting question is how κ behaves at *low* mole fractions of ht. Figure 8 shows a linear decrease in the range

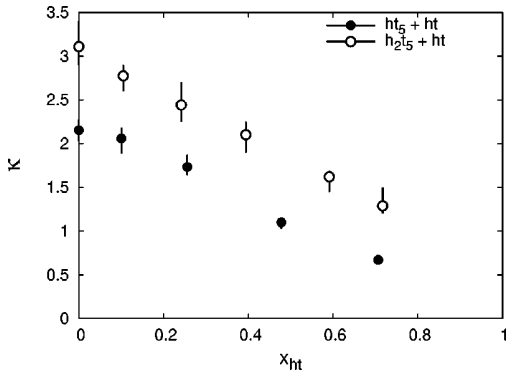

FIG. 8. Bending modulus as a function of mole fraction of cosurfactant added to ht_5 and h_2t_5 surfactants at $\gamma=0.1\gamma_0$.

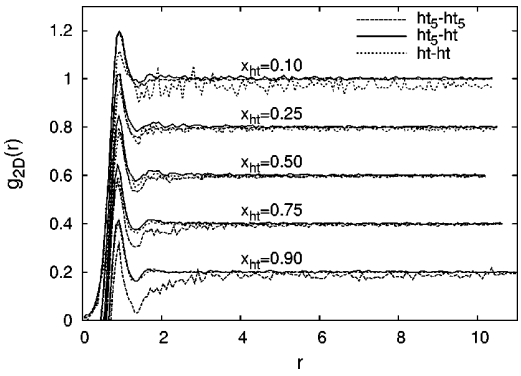

FIG. 10. Two-dimensional radial distribution function for head beads of pairs of ht_5-ht_5, ht_5-ht, and ht–ht molecules for various mole fractions of cosurfactant. Numbers on the y-axis refer to graphs for $x_{ht}=0.10$. Graphs for the other mole fractions have been shifted down by 0.2, 0.4, 0.6, and 0.8, respectively.

of investigation. Mean-field theory at constant area predicts that the film can become very flexible by adding only a small amount of cosurfactant, i.e., a hyperbolic decrease in κ with mole fraction.[16,19] Without the constant area constraint the decrease is linear for $x<0.6$.[17] This is consistent with our results. The available experimental data also supports a linear decrease.[36] It therefore seems that a constant area constraint overestimates the efficiency of cosurfactants in reducing the film rigidity.

We will now discuss the results of Fig. 7 in terms of the chain packing constraints.[16,40] Short molecules acting as spacers between longer molecules reduce the chain–chain repulsion. That is particularly beneficial for a curved monolayer because the available area decreases towards the end of the chain, see Fig. 9. The cartoon shows how the available chain area changes with bending for surfactant molecules of uniform length and for a mixture between short and long surfactants. For those of uniform length, the area per chain segment increases close to the water phase and decreases towards the end of the chain compared to the flat layer. This is also the case for the mixed monolayer, but here this is highly beneficial as the density of chain segments is higher close to the water phase. This explains the difference between the two curves in Fig. 7. Figure 7 also suggests that the effect of the spacers is highest when the mole fractions are roughly equal. A snapshot from the simulation with $x_{ht}=0.5$ was shown in Fig. 3.

To investigate possible ordering in the two-component monolayer we calculated the two-dimensional radial distribution function $g_{2D}(r)$ (Fig. 10). r is here the distance between two surfactant head groups projected onto the interface. Note that the absence of hard-core repulsion between DPD beads allow beads to overlap. Also, there is short-range order but no long-range order. The ht_5-ht_5, ht_5-ht, and ht–ht distributions differ for all mole fractions. This indicates short-range order in the distribution of the two types. The first peak is higher for pairs of different surfactants and the difference increases with decreasing difference in the mole fractions. This indicates a preference for ht_5 molecules to be surrounded by ht molecules and vice versa. This is expected as the entropic repulsion between chains is higher for the surfactants with longer chains, and it supports the packing order shown in Figs. 9(b) and 9(d).

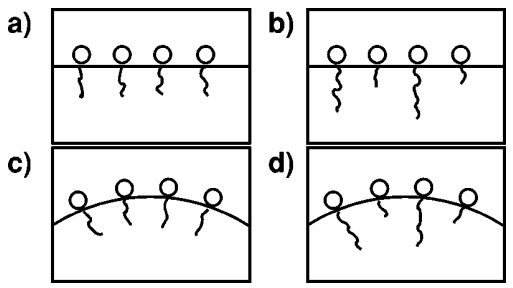

FIG. 9. Cartoon showing medium-length surfactants and a mixture of long- and short-chain surfactants at a planar and curved interface.

D. Linear versus branched surfactants

The difference between linear and branched surfactants with the same number of chain segments is interesting both from a theoretical and practical view point. Previously we reported that these branched surfactants are more efficient than the linear ones in reducing the interfacial tension:[5] At the same area density of surfactants, the branched give a lower interfacial tension. We will now determine the effect of branching on the bending modulus.

We simulated monolayers of the linear surfactant h_2t_5 and the branched surfactant $h_2t(t_2)_2$ at $\gamma=0$ and at $\gamma=0.1\gamma_0$. The results are shown in Fig. 11. The linear surfactant has a higher bending modulus than the branched surfactant. Because the linear one has higher γ for a given density, its packing is denser at a given γ. Due to the double chain of $h_2t(t_2)_2$, we might expect it to have a bending modulus similar to h_2t_2 or h_2t_3 at the same interfacial tension. Given the linear increase in κ with chain length (Fig. 6), the difference between branched and linear surfactants is as expected.

Cosurfactant was added to both linear and branched surfactants. This decreases the difference between the two. It has less effect on the branched surfactant because its double tail already acts as a kind of spacer.

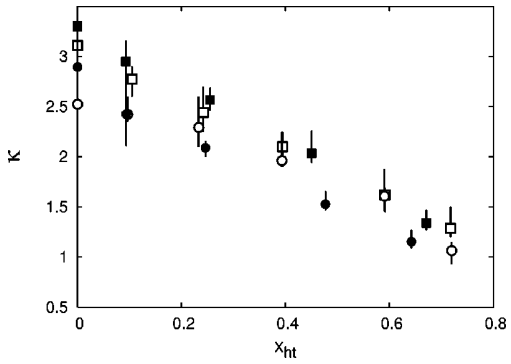

FIG. 11. Bending modulus for linear and branched surfactants as a function of mole fraction of ht surfactant added. The squares denote h_2t_5+ht and the circles denote $h_2t(t_2)_2+ht$. The open symbols are at $\gamma=0.1\gamma_0$ and the solid symbols are at $\gamma=0$.

IV. CONCLUSION

One important result of this paper is that the *thickness* of the layer affects the rigidity more than the *density* of the layer: γ decreases and κ increases with both increasing density and increasing chain length. However, at given γ, i.e., accounted for a difference in density, κ still increases with chain length.

Our simulations are performed at constant low interfacial tension, corresponding to microemulsion monolayers. We calculated values for κ versus chain length for a one-component layer and versus mole fraction of cosurfactant for a binary mixture. The results differ qualitatively from theoretical predictions that assume constant area density. We find that κ increases roughly linearly with chain length for a given head group. This is within the uncertainties of the experiments available, although these are often compared to theoretical predictions at constant area density. With this assumption the chain length increases faster. We also found that mixtures of short and long surfactants are more flexible than medium length surfactants of the same average chain length, but the decrease is roughly linear in mole fraction and less dramatic than without taking the density variations into account.

ACKNOWLEDGMENTS

These investigations are supported in part by the Norwegian Research Council (Grant No. 145184/432), by the Netherlands Research Council for Chemical Sciences (CW), and by the Netherlands Organization for Scientific Research (NWO) through PIONIER.

[1] N. Gov, A. G. Zilman, and S. A. Safran, Phys. Rev. Lett. **90**, 228101 (2003).
[2] S. P. Moulik and P. K. Paul, Adv. Colloid Interface Sci. **78**, 99 (1998).
[3] J. Sjöblom, R. Lindberg, and S. E. Friberg, Adv. Colloid Interface Sci. **65**, 125 (1996).
[4] S. A. Safran, *Statistical Thermodynamics of Surfaces, Interfaces, and Membranes* (Addison–Wesley, Reading, 1994).
[5] L. Rekvig, M. Kranenburg, J. Vreede, B. Hafskjold, and B. Smit, Langmuir **19**, 8195 (2003).
[6] J. N. Israelachvili and H. Wennerström, J. Phys. Chem. **96**, 520 (1992).
[7] D. Langevin, Adv. Colloid Interface Sci. **34**, 583 (1991).
[8] J. Daillant and M. Alba, Rep. Prog. Phys. **63**, 1725 (2000).
[9] R. Goetz, G. Gompper, and R. Lipowsky, Phys. Rev. Lett. **82**, 221 (1999).
[10] E. Lindahl and O. Edholm, Biophys. J. **79**, 426 (2000).
[11] S. J. Marrink and A. E. Mark, J. Phys. Chem. B **105**, 6122 (2001).
[12] G. Ayton and G. A. Voth, Biophys. J. **83**, 3357 (2002).
[13] W. K. den Otter and W. J. Briels, J. Chem. Phys. **118**, 4712 (2003).
[14] M. Laradji and O. G. Mouritsen, J. Chem. Phys. **112**, 8621 (2000).
[15] I. Szleifer, D. Kramer, A. Ben-Shaul, D. Roux, and W. M. Gelbart, Phys. Rev. Lett. **60**, 1966 (1988).
[16] I. Szleifer, D. Kramer, A. Ben-Shaul, W. M. Gelbart, and S. A. Safran, J. Chem. Phys. **92**, 6800 (1990).
[17] R. Cantor, J. Chem. Phys. **99**, 7124 (1993).
[18] R. Cantor, J. Chem. Phys. **103**, 4765 (1995).
[19] S. May and A. Ben-Shaul, J. Chem. Phys. **103**, 3839 (1995).
[20] M. Gradzielski, Curr. Opin. Colloid Interface Sci. **3**, 478 (1998).
[21] M. Venturoli and B. Smit, Phys. Chem. Commun. **2**, 45 (1999).
[22] P. Español and P. B. Warren, Europhys. Lett. **30**, 191 (1995).
[23] R. D. Groot and P. B. Warren, J. Chem. Phys. **107**, 4423 (1997).
[24] P. Prinsen, P. B. Warren, and M. A. J. Michels, Phys. Rev. Lett. **89**, 148302 (2002).
[25] R. D. Groot, Langmuir **16**, 7493 (2000).
[26] R. D. Groot and K. Rabone, Biophys. J. **81**, 725 (2001).
[27] W. Humphrey, A. Dalke, and K. Schulten, J. Mol. Graphics **14**, 33 (1996).
[28] S. M. Willemsen, T. J. H. Vlugt, H. C. J. Hoefsloot, and B. Smit, J. Comput. Phys. **147**, 507 (1998).
[29] G. Gompper, *Soft Matter, Complex Materials on Mesoscopic Scales*, Vol. 10 in *Matter and Materials*, edited by J. K. G. Dhont, G. Gompper, and D. Richter (Forschungszentrum Jülich GmbH, Institut für Festkörperforschung, Jülich, Germany, 2002), pp. B9.1–B9.46.
[30] W. Helfrich, Z. Naturforsch. A **33A**, 305 (1978).
[31] D. Frenkel and B. Smit, *Understanding Molecular Simulations: From Algorithms to Applications*, 2nd ed. (Academic, San Diego, 2002).
[32] S. A. Safran, J. Chem. Phys. **78**, 2073 (1983).
[33] S. T. Milner and S. A. Safran, Phys. Rev. A **36**, 4371 (1987).
[34] M. Gradzielski, D. Langevin, and B. Farago, Phys. Rev. E **53**, 3900 (1996).
[35] C. R. Safinya, E. B. Sirota, D. Roux, and G. S. Smith, Phys. Rev. Lett. **62**, 1134 (1989).
[36] M. Gradzielski, D. Langevin, T. Sottmann, and R. Strey, J. Chem. Phys. **106**, 8232 (1997).
[37] J. Eastoe, D. Sharpe, R. K. Heenan, and S. Egelhaaf, J. Phys. Chem. B **101**, 944 (1997).
[38] C. Guerra, A. M. Somoza, and M. M. Telo da Gama, J. Chem. Phys. **109**, 1152 (1998).
[39] M. Gradzielski, Langmuir **14**, 6037 (1998).
[40] I. Szleifer, A. Ben-Shaul, and W. M. Gelbart, J. Phys. Chem. **94**, 5081 (1990).

Paper IV

Chain Length Dependencies of the Bending Modulus of Surfactant Monolayers

Live Rekvig,[1,*] Bjørn Hafskjold,[1] and Berend Smit[2]

[1]*Department of Chemistry, Norwegian University of Science and Technology, N-7491 Trondheim, Norway*

[2]*Department of Chemical Engineering, University of Amsterdam, Nieuwe Achtergracht 166, 1018 WV Amsterdam, The Netherlands*

(Received 22 October 2003; published 15 March 2004)

The effect of the surfactant chain length n on the bending modulus κ of surfactant monolayers is simulated with a mesoscopic oil-water-surfactant model. We confirm a power law, $\kappa \propto n^p$, as predicted by mean-field theory and found experimentally, and find $p \approx 1.5$ at a constant surface density and $p \approx 1.0$ at a constant interfacial tension. This agrees quite well with both mean-field theory ($p = 2$–3, assuming constant surface density) and experiments (at constant surface tension). Our results suggest that the previously reported agreement between theory and experiment may be fortuitous and caused by the difference in surfactant types.

DOI: 10.1103/PhysRevLett.92.116101 PACS numbers: 61.20.Ja, 68.05.Gh, 82.70.–y

Sufficiently far from a critical point, the properties of an oil-water interface are governed by the interfacial tension. To minimize the surface free energy, the system adopts a configuration that minimizes the interfacial area. Adding surfactant can dramatically change the properties of the interface. Because of their amphiphilic character, surfactant molecules adsorb at the oil-water interface and reduce the interfacial tension. Depending on the surfactant structure, the interfacial tension can become so low that the free energy associated with changes of the curvature of the interface has to be taken into account to understand the properties of the interface [1]. For example, the formation of microemulsion and other phases in surfactant-oil-water systems are explained in terms of the bending modulus which characterizes the free energies of the interface related to changes in the curvature.

Whereas we do have a good understanding of how changes in the surfactant structure influence the interfacial tension, relatively little is known of how these changes affect the bending modulus of the interface. Only recently, the relation between the bending modulus and surfactant chain length has been addressed both experimentally, using high-resolution scattering techniques [2], and theoretically, using mean-field theories [3,4]. On the basis of these theories, the experimental data are interpreted [5–7] with a power-law dependence of the bending modulus κ as a function of the chain length n:

$$\kappa \propto n^p. \tag{1}$$

Mean-field theories predict $p = 2$–3 [1,8], but a recent study shows a strong density dependence [4]. The continuum elasticity theory gives $p = 3$ [1], and experiments indicate $p \sim 3$ [5,6]. However, most experiments measure only the combination $\kappa + \bar{\kappa}/2$ where $\bar{\kappa}$ is the saddle splay modulus [5,6,9].

The mean-field predictions of p are based on comparison of surfactant monolayers of various chain lengths that have the same surface density (N_{surf}/A). Experimentally, it is very difficult to measure or to control the area per surfactant. The experiments have been performed at similar (very low) interfacial tension. This implies that the surface density of surfactant varies with n and therefore these experiments may not be compared directly with the theoretical predictions. This issue motivated us to study the bending modulus of surfactant monolayers using molecular simulations. In this Letter, we introduce a mesoscopic oil-water-surfactant model and use dissipative particle dynamics to compute the effect of changes in the surfactant chain length on the bending modulus both at a given interfacial tension and at a given surface density.

Computing the bending modulus in a molecular simulation is very CPU intensive since one has to analyze the fluctuations of the interface. This requires long simulations on a relatively large system [10]. The height fluctuations in the monolayer can be written in terms of wavelength dependent undulation modes via a Fourier transform. By assuming equipartition, we can relate these undulation modes for small values of the wave vector q to the interfacial tension γ and the bending modulus [1,10],

$$\langle |\tilde{h}(q)|^2 \rangle = \frac{k_B T}{A} \frac{1}{\gamma q^2 + \kappa q^4}, \tag{2}$$

where $k_B T$ is Boltzmann's constant times the temperature and A is the projected area of the interface onto a plane parallel with the interface. This method has been used to compute the bending modulus of a biological membrane [10,11] and a surfactant monolayer [12]. These simulations are important since they demonstrate the feasibility of the method. However, the data are focused on only a few configurations and therefore do not give us sufficient insight into the surfactant chain length dependence to test the theoretical predictions.

In our work, we use a mesoscopic oil-water-surfactant model [13,14] in which oil and water are represented by spherical particles denoted o and w, respectively. A surfactant molecule is constructed by connecting

hydrophilic head particles h and hydrophobic tail particles t with harmonic springs. By changing the number of tail particles, we can study the effect of chain length on the properties of the system. We use dissipative particle dynamics (DPD) to simulate our system. In DPD, we distinguish three types of forces; random forces, dissipative forces, and conservative forces. The random and dissipative forces are chosen such that a canonical ensemble is sampled. We use the conventional forms which have been described extensively in the literature [15]. The conservative forces define the mesoscopic model. We use the commonly used soft-repulsive interaction model [16] to describe the forces between the o, w, h, and t particles:

$$\mathbf{f}(r_{ij}) = a_{ij}\hat{\mathbf{r}}_{ij}\begin{cases} 1 - \frac{r_{ij}}{r_c} & \text{if } r_{ij} < r_c \\ 0 & \text{if } r_{ij} \geq r_c, \end{cases} \quad (3)$$

where r_c is the cutoff radius of the potential, r_{ij} is the distance between particles i and j, and a_{ij} is the repulsion parameter that defines the model. These parameters are chosen such that oil and water particles do not mix and the head and tail particles are hydrophilic and hydrophobic, respectively ($a_{ww} = a_{oo} = 25$, $a_{ow} = a_{oh} = 80$, $a_{wh} = 15$, and $a_{hh} = 35$, with tail particles identical to oil particles). The spring constant and equilibrium length of the harmonic spring connecting the surfactant segments are $k_s = 100$ and $r_0 = 0.7$, respectively. These parameters are based on the work of Groot [16] and have been obtained from a coarse graining procedure that ensure that the water particles at $T = 1$ and $\rho = 3$ reproduce the compressibility of water at ambient conditions. The surfactant parameters have been obtained from a mapping on Flory-Huggins solubility parameters of ionic surfactants, in which one DPD particle typically corresponds to three carbon atoms in the surfactant chain. We use chain lengths that range from 2 to 7 DPD beads corresponding to experimental chain lengths that range from 6 to 21 carbon atoms. Previous studies of monolayers and bilayers have shown that DP models capture essential features of real systems [13,17,18].

Throughout this Letter, we use reduced units; r_c is the unit of length and k_BT the unit of energy. In our simulations we used up to 48 000 particles at $\rho = 3$. The number of surfactants varied from 800 to 1400 and the size of the periodic simulation box was chosen such that the area was approximately 23×23. The equations of motion are solved using the algorithm of Groot and Warren [15] with a time step of 0.03.

In the mean-field theories, the number of surfactants per unit area is input and thus fixed. The simulations are more similar to the experimental situation in the following sense: Water and oil particles separate into two phases. Because of periodic boundary conditions there are two interfaces, but the system is large enough for these to be independent of each other. In contrast to the mean-field approach, the surfactants are not constrained to be at the interface but may leave the interface and form (inverse) micelles in the oil or water phase. Although microemulsions are regarded as isotropic one-phase systems, there are oil rich and water rich regions separated by saturated monolayers on a scale corresponding to our simulation box. A two-phase system with very low interfacial tension is therefore a good representation of a real microemulsion. A typical snapshot of the two monolayers is shown in Fig. 1.

Experimentally, it is also difficult to control the number of surfactants at the interface. The experimental data at various chain lengths refer to different surface densities but to similar (very low) interfacial tensions. To mimic the experimental setup, we also perform simulations in which we impose the interfacial tension. At random intervals in the DPD simulation, we perform a Monte Carlo move in which we change the area of the simulation box in such a way that the total volume of the system remains constant. This attempt to change the area is accepted or rejected with a probability given by

$$\mathrm{acc}(o \to n) = \min(1, \exp\{-[U^n - U^o - \gamma(A^n - A^o)]/k_BT\}), \quad (4)$$

where n and o denote the new and old configuration, respectively, A is the area of the simulation box and U is the total potential energy. In both constant area and constant tension ensembles, we could compute an average density of surfactants at the interface, N/A, by employing a cluster algorithm to decide which surfactants are at the interface [14]. A is the area of the simulation box, or the average box area in the constant tension simulations. The surface tension was computed via the difference in normal and tangential pressure [19]. The surface tension versus surface density equation of state was the same in the two ensembles.

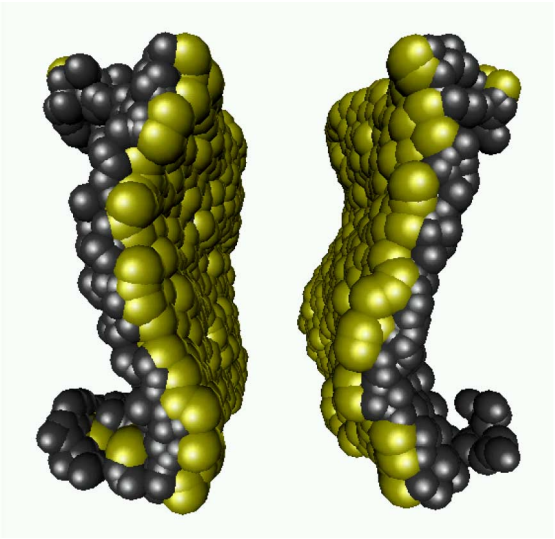

FIG. 1 (color online). Snapshot of two monolayers of ht_4 surfactants at $\gamma = 0$. Head beads are in light gray or yellow and tail beads are in dark gray. Water (in the middle) and oil (on the sides) are not shown.

The height fluctuations of the interface were calculated as in Ref. [14]. Figure 2 shows some typical results of the Fourier analyses. The lines correspond to the fits of Eq. (2) to the results for low wave numbers. The fits give both the interfacial tension and the bending modulus. The data for the interfacial tension correspond nicely to the values that are imposed or computed from the pressure components, indicating that the assumptions behind Eq. (2) are justified. Note that the use of Eq. (2) implies that we assume a zero average curvature of the interface and compute the free energy costs related to deviations from this flat interface. This condition is imposed on the system by the periodic boundary conditions. Experimentally, the asymmetric surfactants that we consider in the simulations may give an interface with a (small) nonzero curvature.

Figure 3 shows the bending modulus for ht_n surfactants ($n = 2$–7) as a function of the surface density 3(a) and interfacial tension 3(b). Although we performed relatively long simulations, the scatter in the data is large, illustrating that the bending modulus is difficult to compute accurately [10]. This makes it difficult to compute the chain length dependence of κ from simulations at a single surface density or interfacial tension. Figure 3 shows that, by systematically varying the surface density and interfacial tension, we can determine the dependence of κ on these properties for various chain lengths. We observe that the bending modulus increases monotonically with the density of surfactants at the interface. Bending the interface becomes increasingly costly because of the packing constraints of the surfactants at the interface. Similar results have been obtained by Laradji and Mouritsen [12].

To determine the chain length dependence at a given surface density or a given interfacial tension, we made linear fits to the results in Fig. 3 for each chain length. From the lines in Fig. 3(a), we computed data points for some densities (shown in Fig. 4, solid symbols). Similarly, the lines in Fig. 3(b) were used to obtain the open symbols in Fig. 4. Each of the data sets in Fig. 4 were fitted to the line $\kappa = a + bn^p$. The solid lines are constant density lines and the dashed lines are constant tension lines. Under both conditions, the bending modulus increases with chain length. However, the behavior is qualitatively different when the monolayers have the same surface density and when they have the same interfacial tension. Equal surface densities give $p = 1.4$–1.6, while equal interfacial tensions give $p = 0.91$–0.98. As the chain length increases, bending the interface becomes increasingly difficult because of packing constraints. However, the surface density will be lower for the longer surfactants at a given interfacial tension. This results in a decrease of the bending modulus, which explains the lower value for p in the case of equal interfacial tensions. In both cases, the exponent is not constant but increases with increasing density and decreasing tension, respectively.

It is instructive to make a more detailed comparison with the experimental data. In our model, a tail bead corresponds to approximately three CH_2 groups of a surfactant tail. The surfactants shown in Fig. 4 correspond

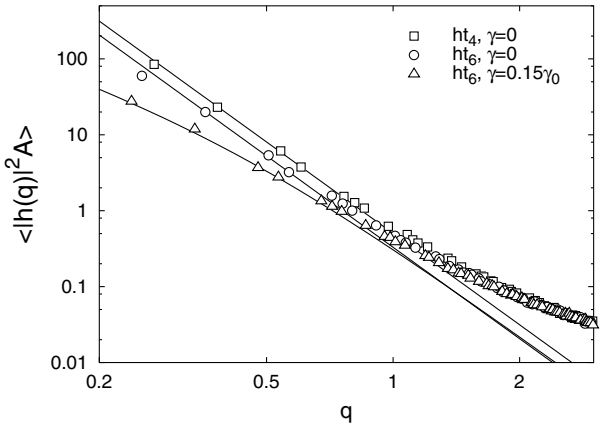

FIG. 2. Fourier spectra for some typical simulations. The lines are fits of the four lowest q values to $1/(\gamma q^2 + \kappa q^4)$, where γ is the imposed surface tension. γ_0 is the bare oil-water interfacial tension.

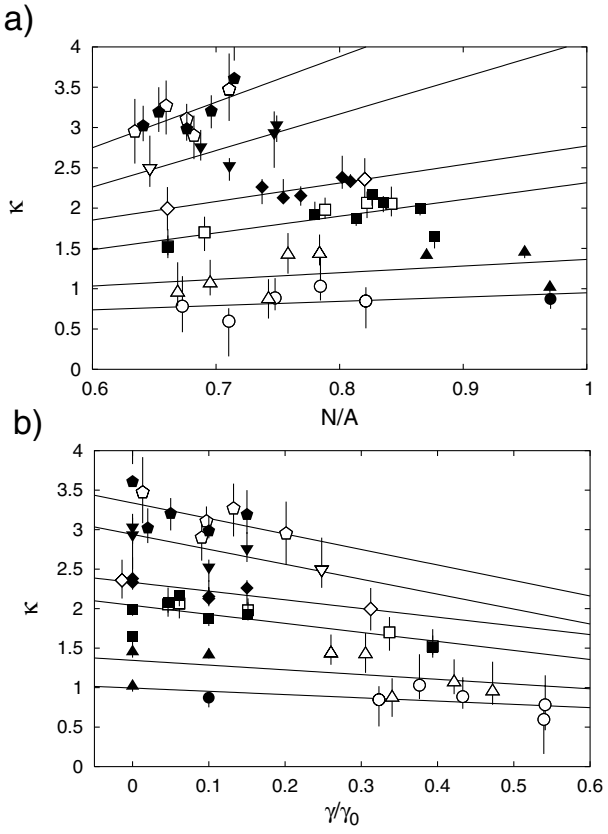

FIG. 3. Bending modulus for ht_n surfactants as a function of surfactant concentration at the interface (a) and interfacial tension (b). ○, $n = 2$; △, $n = 3$; □, $n = 4$; ◇, $n = 5$; ▽, $n = 6$, pentagon, $n = 7$. Open symbols denote data from constant area simulations and solid symbols denote data from constant interfacial tension simulations. The lines are linear fits to the data for each chain length.

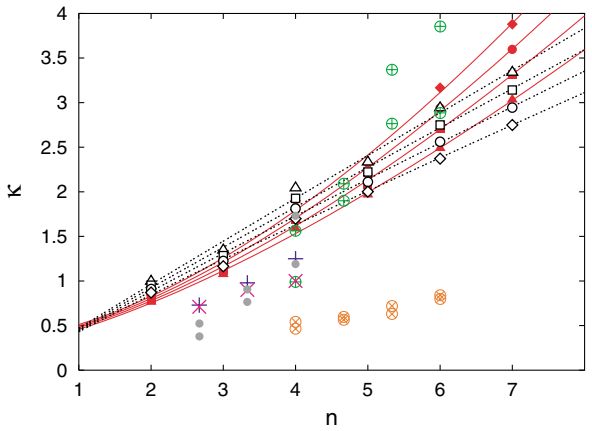

FIG. 4 (color online). Bending modulus as a function of chain length. The solid symbols are for $N/A = 0.65$ (△), $N/A = 0.70$ (□), $N/A = 0.75$ (○), and $N/A = 0.80$ (◇). The open symbols are for $\gamma = 0$ (△), $\gamma = 0.1\gamma_0$ (□), $\gamma = 0.2\gamma_0$ (○), and $\gamma = 0.3\gamma_0$ (◇). The lines are fits to $\kappa = a + bn^p$. Solid lines are constant density lines and dashed lines are constant tension lines. The points are experimental values: ⊕ denotes $\kappa + \bar{\kappa}/2$ for C_iDMAO (amine oxides) from Ref. [6]. ⊗ denotes $\kappa + \bar{\kappa}/2$ for C_i-C_{12} dialkylammoniumbromides from Ref. [9]. + denotes κ for C_iE_4 and × for C_iE_5 (polyethyleneglycol alkyl ethers) from Ref. [20]. ● denotes $\kappa + \bar{\kappa}/2$ for C_iE_5 from Ref. [6]. We used the mapping $n = i/3$.

therefore to chains with 6-21 alkyl units. Experimentally, the bending modulus has been determined for chains with 8-18 alkyl units [5,6,9,20]. In Fig. 4, we plotted data from Refs. [6,9,20] that have three or more chain lengths for a given head group and oil type. It is remarkable that our simple model gives such a good estimate of κ. It reproduces not only the qualitative behavior, but also the order of magnitude (in units of k_BT). Gradzielski *et al.* found $\kappa + \bar{\kappa}/2 \propto n^{2.95}$ [6]. This appears to be in contrast with our simulation, which shows that at constant interfacial tension, $p \approx 1$. However, if we distinguish between data with different head groups, $p \approx 1$ seems to be an equally good estimate also for the experimental data. Accurate data for a wider chain length range would be required to confirm our hypothesis that experiments at constant interfacial tension will yield an exponent that is significantly lower than that predicted by mean-field theories at constant density.

Finally, we remark that also our exponent p at fixed density is lower than the theoretical predictions [1,8]. With three CH_2 groups per bead, $r_c = 6.5$ Å [17] and we get areas per molecule in the range 40–60 Å^2 at $\gamma \approx 0$, depending on the chain length. The theoretical calculations by Würger show that, only at very low surface areas, we would expect $p = 3$ [4]. However, as we study a self-assembled monolayer, such densities are inaccessible in practice.

In this Letter, we have shown that molecular simulations using a mesoscopic oil-water-surfactant system can be used to systematically investigate the effect of changes in the surfactant structure on the bending modulus. We confirm a power-law variation with chain length. However, our simulations indicate that the exponent of this power law depends crucially on the experimental conditions. Since the experiments have been performed at different conditions than for which the theoretical predictions have been made, the apparent agreement of the experimental and theoretically predicted exponent might not hold. Further study is required to determine whether this deviation is related to differences in the models being considered or to the underlying assumptions in the theory.

These investigations are supported in part by the Norwegian Research Council (Grant No. 145184/432), by the Netherlands Research Council for Chemical Sciences (CW), and by the Netherlands Organization for Scientific Research (NWO) through PIONIER.

*Author to whom correspondence should be addressed.
Electronic address: live.rekvig@phys.chem.ntnu.no

[1] S. A. Safran, *Statistical Thermodynamics of Surfaces, Interfaces, and Membranes* (Addison-Wesley, Reading, MA, 1994).
[2] T. Hellweg and D. Langevin, Phys. Rev. E **57**, 6825 (1998).
[3] I. Szleifer, D. Kramer, A. Ben-Shaul, D. Roux, and W. M. Gelbart, Phys. Rev. Lett. **60**, 1966 (1988).
[4] A. Würger, Phys. Rev. Lett. **85**, 337 (2000).
[5] M. Gradzielski, D. Langevin, and B. Farago, Phys. Rev. E **53**, 3900 (1996).
[6] M. Gradzielski, D. Langevin, T. Sottmann, and R. Strey, J. Chem. Phys. **106**, 8232 (1997).
[7] C. R. Safinya, E. B. Sirota, D. Roux, and G. S. Smith, Phys. Rev. Lett. **62**, 1134 (1989).
[8] I. Szleifer, D. Kramer, A. Ben-Shaul, W. M. Gelbart, and S. A. Safran, J. Chem. Phys. **92**, 6800 (1990).
[9] J. Eastoe, D. Sharpe, R. K. Heenan, and S. Egelhaaf, J. Phys. Chem. B **101**, 944 (1997).
[10] R. Goetz, G. Gompper, and R. Lipowsky, Phys. Rev. Lett. **82**, 221 (1999).
[11] E. Lindahl and O. Edholm, Biophys. J. **79**, 426 (2000).
[12] M. Laradji and O. G. Mouritsen, J. Chem. Phys. **112**, 8621 (2000).
[13] L. Rekvig, M. Kranenburg, J. Vreede, B. Hafskjold, and B. Smit, Langmuir **19**, 8195 (2003).
[14] L. Rekvig, B. Hafskjold, and B. Smit, J. Chem. Phys. **120**, 4897 (2004).
[15] R. D. Groot and P B. Warren, J. Chem. Phys. **107**, 4423 (1997).
[16] R. D. Groot, Langmuir **16**, 7493 (2000).
[17] R. D. Groot and K. Rabone, Biophys. J. **81**, 725 (2001).
[18] M. Kranenburg, M. Venturoli, and B. Smit, Phys. Rev. E **67**, 060901 (2003).
[19] D. Frenkel and B. Smit, *Understanding Molecular Simulations: from Algorithms to Applications* (Academic, San Diego, 2002), 2nd ed.
[20] T. Sottmann and R. Strey,J. Chem. Phys. **106**, 8606 (1997).

Paper V

Molecular simulations of surface forces and film rupture in oil/water/surfactant systems

Live Rekvig[1], Bjørn Hafskjold[1], Berend Smit[2]

[1]Department of Chemistry, Norwegian University of Science and Technology
N-7491 Trondheim, Norway
[2] Van 't Hoff Institute for Molecular Sciences, University of Amsterdam
Nieuwe Achtergracht 166, 1018 WV Amsterdam, The Netherlands

Abstract

We use Dissipative Particle Dynamics (DPD) and molecular models to simulate interacting oil/water/surfactant interfaces. The system comprises sections of two emulsion droplets separated by a film. The film is in equilibrium with a continuous phase, in analogy with the surface force apparatus (SFA). This is achieved by combining DPD with a Monte Carlo scheme to simulate a μVT ensemble. The setup enables the computation of surface forces as a function of the distance between the two interfaces, as well as the detection of film rupture. We studied monolayers of non-ionic model surfactants at different densities, and compared oil-water-oil and water-oil-water emulsion films. Between surfactant monolayers facing each other tails-on (water-oil-water films), we observed repulsive forces due to the steric interaction between overlapping hydrophobic tails. The repulsion increases with surfactant density. Conversely, no such repulsion is observed between surfactant monolayers facing each other heads-on. Instead, the film ruptures, the monolayers merge, and a channel forms between the two droplet phases. Film rupture can also be induced in the water-oil-water films by forcing the interfaces together. The separation at rupture increases for oil-water-oil films and decreases for water-oil-water films when the surfactant density increases. The results are in qualitative agreement with existing theories of emulsion stability in creams, in particular with the channel nucleation theory based on the natural curvature of surfactants.

Accepted for publication in *Langmuir*.

This article has been removed from the electronic version of the thesis, but is available in the printed version.